ISTANBUL TECHNICAL UNIVERSITY ★ GRADUATE SCHOOL OF SCIENCE ENGINEERING AND TECHNOLOGY

DESIGN, MODELLING AND CONTROL OF A REACTION WHEEL ACTUATED SYSTEM

M.Sc. THESIS

Rahman Bitirgen

Department of Aeronautical and Astronautical Engineering

Aeronautical and Astronautical Engineering Graduate Programme

December 2018

ISTANBUL TECHNICAL UNIVERSITY ★ GRADUATE SCHOOL OF SCIENCE ENGINEERING AND TECHNOLOGY

DESIGN, MODELLING AND CONTROL OF A REACTION WHEEL ACTUATED SYSTEM

M.Sc. THESIS

Rahman Bitirgen
(511161144)

Department of Aeronautical and Astronautical Engineering

Aeronautical and Astronautical Engineering Graduate Programme

Thesis Advisor: Asst. Prof. Dr. İsmail Bayezit

December 2018

İSTANBUL TEKNİK ÜNİVERSİTESİ ★ FEN BİLİMLERİ ENSTİTÜSÜ

REAKSİYON TEKERİ İLE KONTROL EDİLEN BİR SİSTEMİN TASARIMI, MODELLENMESİ VE KONTROLÜ

YÜKSEK LİSANS TEZİ

Rahman Bitirgen
(511161144)

Ucak ve Uzay Muhendisligi Anabilim Dali

Ucak ve Uzay Muhendisligi Yuksek Lisans Programi

Tez Danışmanı: Asst. Prof. Dr. İsmail Bayezit

Aralik 2018

Rahman Bitirgen, a M.Sc. student of ITU Graduate School of Science Engineering and Technology 511161144 successfully defended the thesis entitled "DESIGN, MODELLING AND CONTROL OF A REACTION WHEEL ACTUATED SYSTEM", which he prepared after fulfilling the requirements specified in the associated legislations, before the jury whose signatures are below.

Thesis Advisor :	**Asst. Prof. Dr. İsmail Bayezit** Istanbul Technical University	.....
Jury Members :	**Asst. Prof. Dr. İsmail Bayezit** Istanbul Technical University	.....
	Asst. Prof. Dr. Cuma Yarım Istanbul Technical University	.....
	Asst. Prof. Dr. İlker Üstoğlu Yıldız Technical University	.....

Date of Submission : **November 16th, 2018**
Date of Defense : **December 25th, 2018**

To my family

FOREWORD

Firstly I would like to thank my advisor Dr. İsmail Bayezit for his continuous support. He helped me whenever I come across a problem which seemed unsolvable at first look. Then we managed to solve, passing through many bottlenecks this research is realized.

I am particularly grateful for the assistance given by my friends Muhsin Hançer, Muhammet Öztürk and Afşin Baran Bayezit.

I would like to express my very great appreciation to my old friend Onur Altınçelik. He helped me on the CAD designs and guided me on manufacturing methods and the type of the materials to choose in the testbed.

I should mention the support of the Scientific Research Council of Istanbul Technical University, for the project named "Reaction Wheel Design, Manufacturing and the Attitude Control of a Spacecraft Actuated by Reaction Wheel Assembly" with the project number of MAB-2017-40957.

Finally, I wish to thank my family for their continuous support and encouragement throughout my study.

December 2018

Rahman Bitirgen
(Astronautical Engineer)

TABLE OF CONTENTS

Page

ABBREVIATIONS

S/C	**:** Spacecraft
RW	**:** Reaction Wheel
RWA	**:** Reaction Wheel Array
MW	**:** Momentum Wheel
CMG	**:** Control Moment Gyroscopes
VSCMG	**:** Variable Speed CMG
DGCMG	**:** Double Gimbal CMG
DGVSCMG	**:** Double Gimbal VSCMG
DC	**:** Direct Current
ESC	**:** Electronic Speed Controller
PWM	**:** Pulse Width Modulation
RF	**:** Radio Frequency
LEO	**:** Low Earth Orbit
PD	**:** Proportional Derivative
CAD	**:** Computer Aided Drafting

SYMBOLS

$\mathbf{M_f}$	**:** Frictional Torque
I, J	**:** Moment of Inertia
b	**:** Frictional Moment Coefficients
t	**:** Time
ω	**:** Angular Velocity
Ω	**:** Angular Speed of the Flywheel

LIST OF TABLES

Page

LIST OF FIGURES

Page

DESIGN, MODELLING AND CONTROL OF A REACTION WHEEL ACTUATED SYSTEM

SUMMARY

The stability and control of spacecrafts has been an significant topic, since the beginning of the space age. The spacecrafts (S/C) can be required to be stable in some missions depending on the requirements. The S/C can also be required to rotate with a given speed, to observe a point in space, to keep its orientation. In these cases, depending on the orbit of the S/C, the attitude of the S/C should be changed with an active control method.

The attitude control of a S/C can be realized with active and/or passive methods. Spin stabilization is a passive method and used for the control of some S/C in the beginning of the space age. This method utilizes the gyroscopic rigidity of a spinning object to reject the disturbances on the rotating axis. Gravity gradient stabilization is another passive stabilization technique. In this method, the S/C should be longer in one axis comparing it to the other axis. The gradient in the length causes the gradient in the gravity. In this way, the longest axis is aligned with the gravity vector and stability can be maintained through the orbit. However the S/C can rotate freely about the gravity axis, due to no control effort on that axis. Therefore it is not suitable for precise missions.

In active methods, the attitude of the S/C can be changed with actuators. Magnetic torquers are used to exert a moment on the S/C by applying a current on an inductor. They can be used to dump the excess momentum of the momentum exchange devices. Thrusters can be used in the orbit transfers due to their high torque/force output. They can be used to apply high angle maneuvers on the S/C, also the momentum dumping operations can be done using thrusters. Momentum exhange devices uses the reaction torque generated when the speed or the rotating axis of a high inertia flywheel is changed. Reaction wheel (RW) is composed of a flywheel, an electric motor to drive it and electronic components to change the voltage/current applied on the motor in order to change the speed of the flywheel. Control moment gyroscopes (CMG) can be considered as a RW attached to a gimbal, and on that gimbal axis there is a high torque capable electric motor. The rotation axis can be changed by this gimbal and high control moments comparing to the RW, can be achieved by CMGs. RWs and CMGs are used in high precise missions. CMGs are more complex than the RWs and they are much more expensive. Depending on the mission requirements an active or a passive method and proper actuators can be chosen.

In this thesis, reaction wheels, their electro-mechanical structure is researched. A literature survey is conducted on RWs and the control applications with RWs. In the literature, it is observed that most of the research is done on computer simulation environment. It is important to test the systems both mechanical and electronic, on a realistic test environment before real operations. On a test system, the sensors and

actuators can be tested and a possible failure can be prevented beforehand. In this research, for the purposes of modelling an control, a RW and a RW actuated test system is designed on computer aided drafting (CAD) programme and then manufactured. As a result, it become possible to observe the behavior of this dynamic system. A mathematical model is developed and validated with the experimental data. Then, the desinged controller is tested on the platform.

In the first section, the current research in the literature is presented. The purpose of the thesis is explained.

In the second section, the design process of RW and the test platform is explained with the CAD drawings. The testbed can be rotated in two axis, pitch and yaw. On each axis, there is a RW to control the orientation. There are encoders on each axis to measure the angles. The measured angles are processed with a controller and the control signal is applied on the RWs. The processes of measurement, calculation, data recording, controller implementation are done on a micro-controller.

In the third section, the mathematical model for a RW and the testbed is obtained. RW is modelled using DC motor model. The testbed is modelled with the Newton's second law, the friction is taken as viscous friction and embedded in the equation of motion. During tests, it is observed that the simulation results and the real data does not match. An update for the friction model is required. Literature is surveyed on the topic of friction. It is decided that the Stribeck friction model best represent the nonlinear behavior of the testbed.

In the fourth section, controllers are designed. The first one is an open loop control law to determine the time when to increase speed of the flywheel and when to decrease it. In order to check if the desired angle is reached a feedback controller is needed. The second controller is A PD based controller designed using parameter space approach.

In the last section, the contribution of the thesis is explained briefly and future work is discussed.

REAKSİYON TEKERİ İLE KONTROL EDİLEN BİR SİSTEMİN TASARIMI, MODELLENMESİ VE KONTROLÜ

ÖZET

Uzay çağının başladığı zamandan günümüze, uzay araçlarının kararlılığı ve kontrolü önemli bir konu olarak gelişimini sürdürmektedir. Uzay araçları kendileri için belirlenen görevleri gerçekleştirmeleri için kararlı bir yönelme halinde olmaları beklenebilir. Örneğin sürekli dönen bir uydu ile iletişim kurabilmek için, uydunun üzerinde çok yönlü ve çok sayıda anten olması gerekir, ancak eğer uydu sürekli nadir doğrultusunda bakacak şekilde kararlı hale getirilirse tek bir anten ile iletişim sağlanabilir. Benzer şekilde, uzay aracının belirli bir noktaya yönelmesi beklenebilir, örneğin derin uzay araştırmaları, gezegen gözlemleri vb. Bunun gibi durumlarda uzay aracının yörüngesine de bağlı olarak, aktif bir kontrol yöntemi ile yönelmesinin değiştirilmesi gerekmektedir.

Uzay araçlarının yönelme kontrolü aktif ya da pasif olarak gerçekleştirilebilmektedir. Pasif yöntemlerden uzay aracının belirli bir hızda döndürülmesi ile kararlı hale getirilmesi yöntemi ilk uzay araçlarında kullanılan bir yöntemdir ve jiroskopik etkiden yararlanılarak dönme ekseninde oluşan bozucu etkilerin giderilmesini sağlar. Bu yöntemde düşük hassasiyet ile kararlılık sağlanır ve haberleşme için çok yönlü antenler kullanılmalıdır. Yer çekiminin değişiminden faydalanarak da pasif olarak uzay aracının kararlı hale getirilmesi mümkündür. Bunun için aracın boyunun eninden çok daha uzun olması gerekmektedir. Bu hali ile uzay aracı bir sarkaca benzetilebilir. Aracın yere yakın bölümüne daha fazla ağırlık kuvveti etkiyor iken, uzak tarafına daha az ağırlık kuvveti etkiyecektir. Oluşan bu fark ile uzay aracının uzun olduğu eksen ile nadir doğrultusunun çakışması sağlanır. Yüksek hassasiyetli uygulamalar için uygun değildir.

Aktif yöntemlerde ise kullanılan bir eyleyici ile aktif olarak yönelme kontrolü sağlanabilir. Manyetik eyleyiciler ile bobin üzerinden akım geçirilmesi sonucu bir moment elde edilip yönelme kontrolü sağlanabilir. Ayrıca diğer bir eyleyici olan momentum değişim cihazlarında bulunan disklerin limit hıza erişmeleri halinde kontrollü olarak yavaşlatılmalarında kullanılabilirler. İtki sistemleri yörünge transferlerinde kullanıldığı gibi, yönelme kontrolünde de kullanılabilirler, kimyasal, soğuk gaz ve elektrik olmak üzere üç alt gruba ayrılabilirler. Kimyasal itki cihazları yüksek kuvvet/moment üretebildikleri için momentum değişim cihazlarının yavaşlatılmasında kullanılabilirler. Ayrıca hızlı ve büyük açılı bir yönelme manevrasında kullanılabilirler. Elektrik ve soğuk gaz itki cihazları görece daha düşük kontrol momenti üretirler ve yönelme manevralarında kullanılırlar. Buraya kadar anlatılan aktif kontrol yöntemleri dış bir etki ile moment oluştururlar, momentum değişim cihazlarında ise uzay aracının içinde bir diskin dönüş hızının ya da dönme ekseninin değiştirilmesi bir tepki momenti elde edilir. Reaksiyon Tekerleri (RW), Momentum Tekerleri ve Kontrol Moment Jiroskopları şeklinde üç ayrı grupta toplanabilir. Reaksiyon tekerleri ve momentum tekerleri yapısal olarak aynıdır ancak

çalışma prensipleri itibari ile farklılık gösterirler. Bu eyleyiciler, yüksek ataletli bir disk, bu diskin döndürülmesini sağlayan bir elektrik motoru ve motora giden akımı ve gerilimin ayarlanmasında kullanılan devreden oluşurlar. Momentum tekerleri sabit bir hızda döner ve oluşan jiroskopik etki ile kararlılık sağlanır. Reaksiyon (Tepki) tekerlerinde ise diskin dönüş hızı değiştirilerek bir tepki momenti elde edilir. Kontrol Moment Jiroskopları (CMG) ise reaksiyon tekerinin dönüş eksenine gimbal eklenmiş hali olarak düşünülebilir. Bu gimbal ekseninde yüksek tork sağlayabilen bir motor bulunur. CMG'lerde dönen disk sabit hızda dönebileceği gibi, reaksiyon tekeri gibi değişken hızlarda da dönebilir. Gimbal eksenine bağlı olan motorun çalıştırılması ile momentum vektörünün yönü değiştirilir ve RW'ye kıyasla yüksek bir kontrol momenti elde edilebilir. Yüksek hassasiyet gerektiren görevlerde, örneğin uzay teleskopunun belirli bir hızda dönüp, belirli bir noktaya bakması ve sabit olarak o noktaya bakıyor vaziyette kalması gibi, RW ve CMG'ler kullanılırlar. CMG, RW'ye göre daha kompleks bir yapıdadır ve daha maliyetlidir ancak daha yüksek kontrol momenti üretebilir. Uzay görevine bağlı olarak aktif ya da pasif bir yöntem belirlenerek, görevin gereklerini karşılayacak eyleyici(ler) seçilebilir.

Bu çalışmada, reaksiyon tekerleri incelenmiş, mekanik-elektronik yapısı konusunda araştırmalar yapılmış, RW'ler ile uzay aracının kontrolü konusunda yapılan yayınlar taranmıştır. Yapılan yayınlarda genellikle kontrol yöntemleri anlatılmış ve simülasyon sonuçları verilmiş, gerçek bir senaryoda ya da donanımsal bir benzetim ortamında test edilmemiştir. Modelleme ve kontrol açısından bakıldığında donanımsal benzetim ortamı, gerçek testler gerçekleştirilmeden önce ve bilgisayar simülasyonlarından sonra önemli bir yer teşkil etmektedir. Test sistemi ile kullanılan eyleyiciler gerçeğe yakın senaryolarda test edilebilir, oluşabilecek hata durumları önceden fark edilip giderilebilir. Bu çalışmada modelleme ve kontrol işlemlerini gerçekleştirmek amacıyla reaksiyon tekeri mekanizması ve reaksiyon tekeri test mekanizması mekanik ve elektronik olarak tasarlanmış ve üretilmiştir. Bu sayede uzay araçlarında da kullanılan dinamik bir sistemin davranışı gözlemlenmiş ve matematiksel modellemesi ve fiziksel parametrelerinin belirlenmesi işlemleri gerçekleştirilmiştir. Sonraki aşamada ise test mekanizması üzerinde, tasarlanan yönelme kontrolörü test edilmiştir.

Birinci bölümde konuya giriş yapılmış, literatüre atıf yapılarak hangi konuların çalışıldığı belirtilmiştir. Konunun neden seçildiği ve tezin amacı detaylı bir şekilde anlatılmıştır.

İkinci bölümde teker tasarımında nasıl bir yol izlendiği, tasarımların hangi değişikliklerden geçtiği, bilgisayar destekli çizim ortamında hazırlanan çizimler eklenerek anlatılmıştır. Tasarlanan test düzeneği yunuslama ve sapma eksenleri etrafında hareket edebilmektedir. İki eksende de kontrolü sağlamak için birer RW bulunmaktadır. Eksenlerdeki dönüş açıları enkoderlar ile ölçülmektedir. Enkoderlardan gelen yönelme açıları tasarlanan kontrolörde işlemden geçerek RW'lere iletilmekte ve kontrol sağlanmaktadır. Veri işleme, kaydetme ve kontrolör implementasyonu işlemleri bir mikrokontrolcü ile gerçekleştirilmektedir.

Üçüncü bölümde RW ve test sisteminin matematiksel modelinin nasıl elde edildiğinden bahsedilmektedir. RW, doğru akım motor modeli kullanılarak modellenmiştir. Farklı gerilimler için diskin sahip olduğu hızlar kaydedilmiş, motor üreticinin verdiği motor ile ilgili parametreler kullanılarak simülasyon gerçekleştirlmiş ve model, yapılan ölçümler ile doğrulanmıştır. Test sistemi ise Newton'un ikinci yasası kullanılarak modellenmiş, eksenlerdeki sürtünmeler viskoz sürtünme olarak

denklemlere dahil edilmiştir. Bu aşamada yapılan ölçümler ile matematiksel modelin simülasyonu birbirleri ile eşleşmemiştir. Bunun sebebi olarak düzeneğin sürtünmesinin doğrusal bir davranış göstermemesi olarak görülmüştür. Bu noktada, test sisteminin modellemesini daha sağlıklı yapabilmek için literatürde bulunan sürtünme modelleri incelenmiş ve statik sürtünmeyi de içeren Stribeck modelinin uygun olduğu görülmüştür. Yapılan ölçümlerden elde edilen veriler, tezde anlatılan yöntemden geçirilerek sürtünmeyi belirleyen parametreler kestirilmiştir. Elde edilen yeni model farklı verilerde de test edilmiş ve yeni modelin ölçümlere yakınsadığı görülmüştür.

Dördüncü bölümde, tasarlanan iki farklı kontrol yöntemi anlatılmıştır. Bunlardan ilki, sistem dinamiğinin baştan çözdürülerek, hangi anda diskin hızlandırılacağının hangi anda diskin yavaşlatılacağının bulunması prensibine dayanmaktadır. Bu yöntem açık çevrim kontrol yöntemi olarak adlandırılabilir, geri besleme kullanılmamaktadır. Ancak, sistemin yönelmesinin istenilen değerlere gelip gelmediğini anlamak için geri beslemeli bir yöntem kullanılmalıdır. Tasarlanan ikinci yöntemde, kontrolör parametreleri sistem transfer fonkiyonuna belirsiz parametreler olarak girilmiş, bu parametreler belirli bir uzayda taranarak, kararlılığı sağlayan kazanç değerleri bulunmuştur. Simulasyon sonuçları ve test sistemi sonuçları sunulmuştur.

Sonuç bölümünde ise tezin katkısı ve gelecekte yapılması planlanan çalışmalardan bahsedilmişitr.

1. INTRODUCTION

The exploration of space has been a topic of interest for a century. Once was a dream for humanity, now capable of reaching at the edge of solar system and observing beyond. The capability of sending payloads to orbit Earth, spacecrafts needed to be controlled to be stable and/or to be oriented. Initially, the S/Cs were to be controlled by passive methods such as spin stabilization or gravity gradient stabilization. Later on, active stabilization became a requirement for some missions such as low earth orbit (LEO) observation satellites. The active methods consist of gas thrusters, magnetic torque rods, momentum exchange devices. These actuators and their variations are used depending on their cost, advantage/disadvantage for the mission in question. Gas thrusters are used to change the orbit of the satellite since they have high force/torque capabililty. They are used to change the attitude of the S/C, however their bandwidth is not wide as other actuators, because they only work in an on/off manner. The momentum dumping feature of these actuators are used to dump the excess momentum of RW and CMGs.

Magnetic torque rods are used in the orbits of planets with magnetic field, and in the effective range of this magnetic field. They need electricity to be actively used. Their bandwidth is wide, however the output torque is low.

Momentum exchange devices use the angular momentum difference to generate control torque for attitude control. They can be classified in two categories, first Reaction Wheels (RWs) and Control Moment Gyroscopes (CMGs). A RW has an electric motor, a flywheel driven by the motor and electronic components to change the speed of the flywheel. A S/C can be controlled by RW Array (RWA) by changing the speed of the flywheels. A CMG has the same components as a RW, in addition it has a torque motor to change the angular momentum vector of the flywheel. This amplifies the torque as an advantage for the CMG. CMGs can be modified into Variable Speed CMGs (VSCMGs), by changing the speed of the flywheel, it combines the RW effect and the CMG torque amplification. This also helps to escape singularities that

can be caused by gimbal lock. CMG can be furhter modified into a Double Gimbal CMG (DGCMG) which has a higher torque amplification capability. The complexity and cost from RW, CMG, SGCMG to DGCMG increases.

A RW is advantageous actuator to orient the S/C from one attitude to another, since it requires no fuel, it can run wherever the S/C can generate electricity. It has high bandwidth comparing it to gas thrusters. It has low complexity comparing it to CMGs.

In the starting phase of this thesis, the literature for momentum exchange devices are searched. The advantages of RWs made them the topic of this thesis. They are low complexity electro-mechanical devices and they can be manufactured and controlled by low cost microcontrollers.

In this thesis, mathematical model for a RW is obtained and validated. Also, in 1DOF and in 2DOF configurations the RW actuated systems are designed and manufactured. The main purpose is to obtain a mathematical model for these systems, identify the physical parameters, and finally validate the model. The last part is to design controllers to change the attitude of the test systems.

1.1 Purpose of Thesis

There have been significant contribution in the literature of control theory and in the spacecraft control applications, however some of these contributions cannot have place to be tested on the spacecraft itself or even on a test environment. In this thesis, a model is developed and validated with the experimental data for a reaction wheel and reaction wheel actuated system. The purpose of this thesis is to develop and validate a momentum exchange system and to be able to test new control methods.

1.2 Literature Review

The momentum based control of spacecraft, with active or passive methods, dates back to the beginning of the space age. In the first applications, the S/C is rotated with an angular rate, this passive method utilizes the gyroscopic rigidity of a rotating object [1].

In later studies, the spacecraft is designed to be composed of two parts as rotor and stator and with the angular momentum of the rotating part, the system is kept stable. With the development of technology, reaction wheels and control moment gyroscope

devices have been used to generate momentum by rotating one or more discs or changing rotation axes instead of rotating the entire spacecraft. The reaction wheels are based on the principle of producing reaction torque by changing the speed of the wheel. With this reaction torque produced, the spacecraft can perform the desired orientation movement in three axes. The most common state of a rotating disk and the control torque is the variable speed control moment gyroscopes (VSCMG)). In these devices, the direction of angular momentum can be changed by the motor on the gimbal axis. These devices can produce higher torques than the reaction wheels, but they are more complex and have higher costs. Table 1.1 shows the comparative table of the actuators used in the orientation control.

Table 1.1 : Comparison of Attitude Control Actuators [1]

Actuators	Typical attitude-control applications	Agility ratio rate/acc (seconds) (smaller ratio is more agile)	Precision (deg)	ACS control bandwith (Hz)	Torque/power (Nm/W)
Spin stabilization	Low-precision omnidirectional RF payloads and magnetospheric science	N/A	0.1-1 in 2 axes	N/A	N/A
Gravity-gradient boom	Coarse earth observation and technology demonstrations	N/A	5-20 in 2 axes	N/A	N/A
Magnetic torquers	Momentum dumps, nanosatellites in LEO, gravity-gradient augmentation	Low agility	1-10 in 2 axes	0.01-0.1	0.001-0.01
Momentum Wheels	Astronomy, communications	N/A	0.001-1 in 3 axes	0.01-0.1	0.001-0.01
Reaction Wheels	Astronomy, communications, earth observation	5-500	0.001-1 in 3 axes	0.01-1	0.001-0.1
Control-moment gyros	Earth imaging and radar, nanosatellites in LEO, gravity-gradient augmentation	0.5-5 (most agile)	0.001-1, in 3 axes, or better	0.1-1	1-10
Electric thrusters	GEO stationkeeping	Low agility	0.01-0.1, in 3 axes	0.001-0.01	0.0001-0.001
Chemical thrusters	Missile defense, interplanetary transfer, spin-speed adjustment and reorientation, momentum dumps	High agility	1-10, in 3 axes	0.1-1	Very high

We can collect the studies on reaction wheels in the following topics: zero speed crossing [1] [3], minimum time optimal control [4] [5], integrated momentum storage and orientation control system [6] [7] [8] , the reaction wheel array configuration [9] [10], the vibration generated in the spacecraft [7] [11], the momentum discharge [12], and applications outside the spacecraft [13] [14] [15]. Thanks to this detailed literature survey, it is possible to take into consideration the configuration trials and the optimal and linear controller tests that are expected to be realized in the thesis. Studies have been carried out to determine which configuration will provide the lowest power consumption for different tasks in configuration [9]. In another study [10], it was explored how the torque and momentum envelopes should be positioned in order to provide optimal agility, and how torque and momentum should be distributed between the wheels. It is also important that the spacecraft performs the steering maneuver in the shortest time and with the lowest power consumption. In this regard; in the operation [4], the reaction time of the reaction wheels to the maximum speed and the time from the maximum to the stationary position are known. In order to perform the eigenvector rotation, the equation of motion is analytically solved and the open loop control law were calculated. In ref. [5] it is developed a control law that defined energy as a function and minimized it. With the knowledge gathered in the literature research section of the thesis, information about how the system requirements should be taken, what should be paid attention to in the wheel design, and which control methods can be used to control the RWA in the following stages are obtained.

2. DESIGNING A REACTION WHEEL AND A REACTION WHEEL ACTUATED SYSTEM

In this chapter, design methodology for a reaction wheel surveyed in the literature. Furthermore, in order to apply a reaction wheel test on ground, initial simulations are carried out. In the first phase, the requirement for a RW is considered, how fast the RW should rotate the test system, what the inertia of the testbed is, etc. Next, based on the literature, a design method is utilized to determine the size of the RW. This method, however, is to be applied for a S/C, for ground applications, there are significant effects, such as friction, mass imbalance on the rotation axes.

2.1 Determining the Wheel Dimensions

In this section, using the methodology described in [16], the dimensioning of the flywheel according to the determined time and rotation angle is explained.

Depending on the specific parameters of the reaction wheel and spacecraft, the moment of inertia of the wheel may be determined. The maximum speed at which the motor and the disc can rotate:

$$\Omega_{max} = 4000\ rpm \tag{2.1}$$

J is the moment of inertia of the flywheel. Maximum angular momentum that the wheel can have:

$$h_{max} = J\Omega_{max} = J * 4000 * \frac{2\pi}{60} \tag{2.2}$$

In order to rotate the S/C, an angle of θ

$$t_f = \frac{2I_{max}\theta}{h_{max}} \tag{2.3}$$

I_{max} Here is the maximum moment of inertia of the I_{max} spacecraft or testbed. Some of the limitations of the wheel can be added to the equation, the moment of inertia can

Figure 2.1 : Model Lab 3DOF Gyroscopic Test Mechanism. [2]

be found, and the number of times it will be able to perform a maneuver, or otherwise, the inertia of a wheel that can perform the desired maneuver within a set time can be found. The first way was used here, primarily the diameter of the wheel is not to exceed 10cm. This can be explained by the limited size of the testbed in Figure 2.1 and the power requirement. The testbed seen in Fig. 2.1 will be used in the scope of the project mention in the Foreword section. The RW and testbed used in the thesis is funded by the same project and the same RWs will be tested on the gyroscopic test platform seen in Fig. 2.1 in future studies, therefore the maximum possible inertia is the yaw inertia of the gyroscopic test platform seen in Fig. 2.1 and it is taken in the calculations. The moment of inertia of the ring can be calculated analytically when its wheel is considered as a ring and its material properties are known. The outer radius of the ring can be taken as R = 10cm inner radius r and the thickness of the disk can be taken as d and the volume of the ring can be calculated. Aluminum is considered as the material of the wheel. The mass can be calculated using the volume and density information, and the moment of inertia can be found here. Cross-sectional area of the ring:

$$A = \pi \left(R^2 - r^2\right) \tag{2.4}$$

Volume of the ring:

$$V = A \times d \tag{2.5}$$

Mass of the ring

$$m = \rho V \tag{2.6}$$

Inertia of the ring:

$$J = mR^2 \tag{2.7}$$

These equations are coded parametrically in MATLAB. By changing the r and d values, the moment of inertia can be increased or decreased for the same diameter wheel. When $R = 5\ cm$, $r = 4\ cm$, $d = 0.5\ cm$, a 90 degree rotation can be done in 15 seconds for the specified characteristics.

2.2 Designing Reaction Wheel

In the literature, the topics of the papers are mostly about the controller design, stability analysis etc. However, they are mostly based on simulations assuming the RW performs without any imperfections. There are not so much detail about the manufacturing of a RW.

The components of the RW are a motor and its driver, a flywheel, an encoder to measure the speed, and a box to hold these together and to prevent the damage in a case of failure. In Fig. 2.2, initial design of the RW is presented as exploded assembly form. In Fig. 2.3 cross section view of the designed RW can be seen.

In the next design iteration, it is decided to be able to change the motor and the flywheel to analyze the performance of different motors and flywheels. This also will help to validate the model parameters of the RW. A plate is designed and mounted on the CAD drawing, also 3 options for flywheels are included. This new design can be seen in Fig. 2.4.

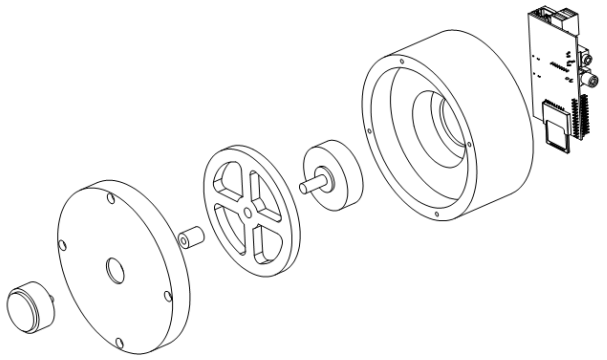

Figure 2.2 : Reaction Wheel (Encoder, Flywheel, Motor and its Driver) Initial Design

There should be a speed measurement equipment to keep the speed of the wheel constant when control torque generation is not required. An encoder is thought to be mounted on the RW. However, the encoder to be used is limited to the maximum speed of 1000 rpm. In order to solve this problem, tests are performed on the RW to identify the behaviour of the RW, within the safe operational speed range. In normal operation, the encoders will not be used.

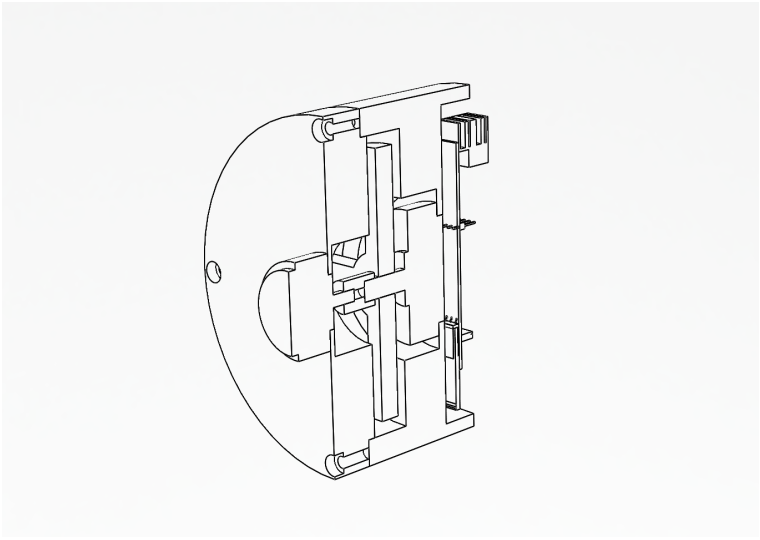

Figure 2.3 : Reaction Wheel Cross Section

2.3 Designing a Reaction Wheel Actuated System

In order to test the torque capability of the RWs, to test the controllers on the RWs, to test how the RWs can actuate a system, a testbed is required. The literature is

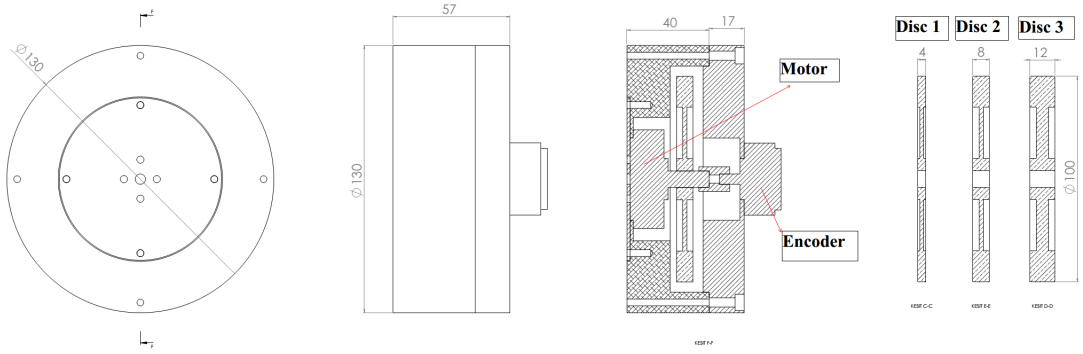

Figure 2.4 : Reaction Wheel Components and Disc Options (Final Design)

sureveyed on this subject, testbed manufacturers, their products are examined. The proposed design is a two degree of freedom reaction wheel actuated system. This system has a base on which the moving parts are mounted. It can freely rotate on the yaw axis without restrictions, on the pitch axis, it can rotate in a range between -40 degrees and 40 degrees. The final design on a CAD program can be seen in Fig. 2.5. Previous designs can be seen in the figures in the appendices section.

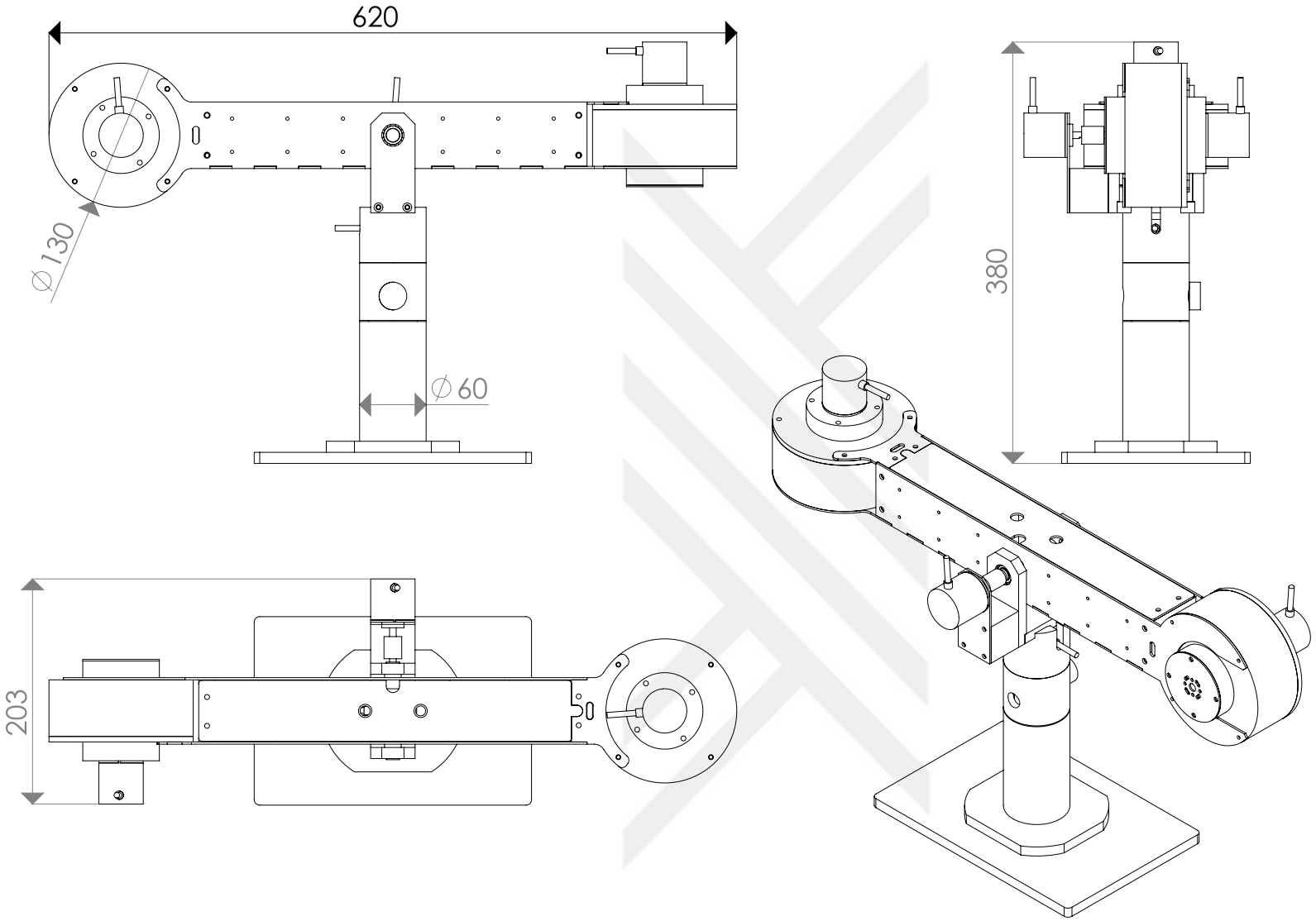

Figure 2.5 : The 2DOF RW Actuated Testbed Final Design.

The main requirements in the design process were:

- to be easily manufactured
- to have less number of components, less complex
- easy to mount the RWs
- to be as small as possible, in weight and in dimensions
- to be able to mount the encoders to measure the angle
- to have small amount of friction

These design concerns are taken into account and the testbed is designed in CAD environments, several revisions are made until the final version is reached.

The testbed is manufactured and components are assembled as seen in Fig. 2.6

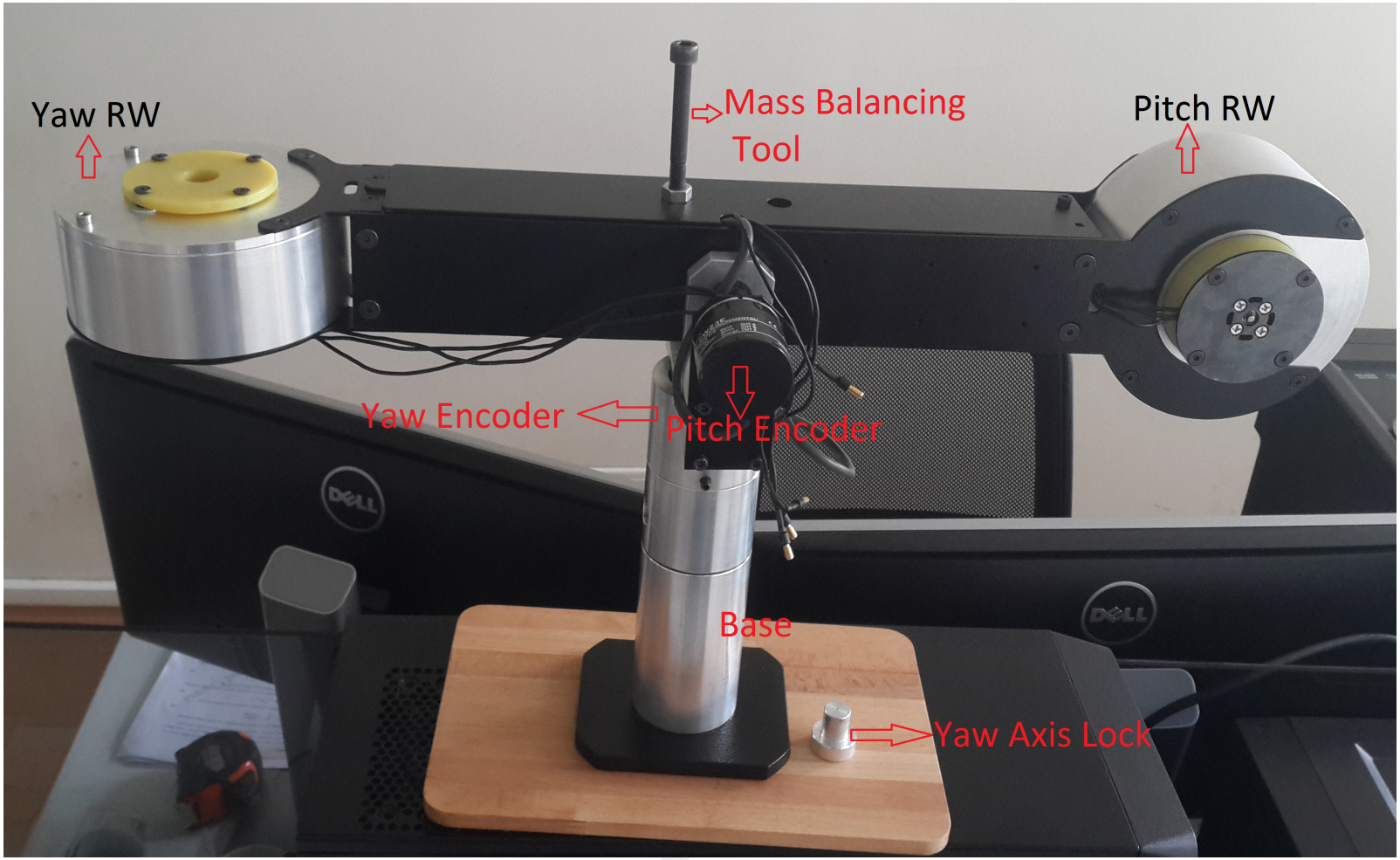

Figure 2.6 : The 2DOF RW Actuated Testbed

As seen in Fig. 2.6, the testbed can rotate around two axes, pitch and yaw. It has two reaction wheels to be able to control the orientation with the reaction torque generated by the RWs. It has two encoders to measure the pitch and yaw angle.

3. MODELLING A REACTION WHEEL AND A REACTION WHEEL ACTUATED SYSTEM

In this chapter, in order to simulate the behaviour of the system, a model is developed. First the reaction wheel is modelled with the well-known DC motor model and the physical parameters are either given by the manufacturer or identified. The RW actuated system equations are derived using Newton's second law. The inital viscous friction model was not representing the behaviour of the system. Therefore a new model is proposed based on the literature.

3.1 Modelling Reaction Wheel

Reaction wheel is simply an electric motor and a flywheel driven by it. The high inertia flywheel helps to generate torque when it is accelerated by manipulating the voltage on the motor. Direct current electric motor mathematical model is utilized, the wheel inertia is included.

3.1.1 DC Motor Model

The DC Motor model including the rotor inertia:

$$\begin{aligned} J\dot{\Omega} + b\Omega &= Ki \\ L\frac{di}{dt} + Ri &= V - K\Omega \end{aligned} \tag{3.1}$$

The parameters in the equations are given in Table 3.1.

Table 3.1 : Motor Parameters.

Parameter	Explanation	Value	Unit
J	Wheel Inertia	1.24e-4	kgm^2
R	Motor Resistance	0.83	ohm
L	Motor Inductance	0.0641	H
b	Motor Friction Coefficient	4.07e-6	Nms/rad
K	Motor Torque Constant	0.0182	Nm/A

The parameter J is the inertia of the wheel and it is modelled in CAD programme, its inertia is taken from this programme. R is the motor resistance and L is the motor

inductance, these values are taken from the datasheet of the manufacturer. However b which is the motor friction is not given in the datasheet, this parameter is identified as follows: first measurements are taken on the system, for a certain voltage applied on the motor, the terminal speed of the wheel is recorded.

When there is no change in the speed of the wheel and the current is constant in the steady state, the equations become:

$$\begin{aligned} b\Omega &= Ki \\ Ri &= V - K\Omega \end{aligned} \tag{3.2}$$

Solving the equations above

$$\left(\frac{Rb}{K} + K\right) = \frac{V}{\Omega} \tag{3.3}$$

Limit speeds for the wheel is recorded for some certain voltage values.

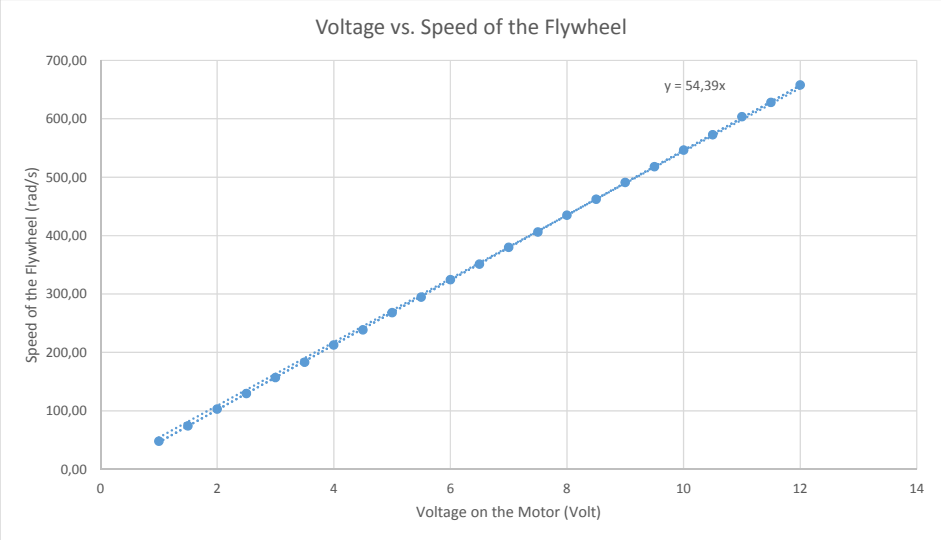

Figure 3.1 : The Relation Between the Limit Speed of the Flywheel and the Voltage on the Motor

The equations 3.1 are solved numerically with the given parameters in Table 3.1. The angular speed of the flywheel and the current that is drawn by the motor can be seen in Fig. 3.2.

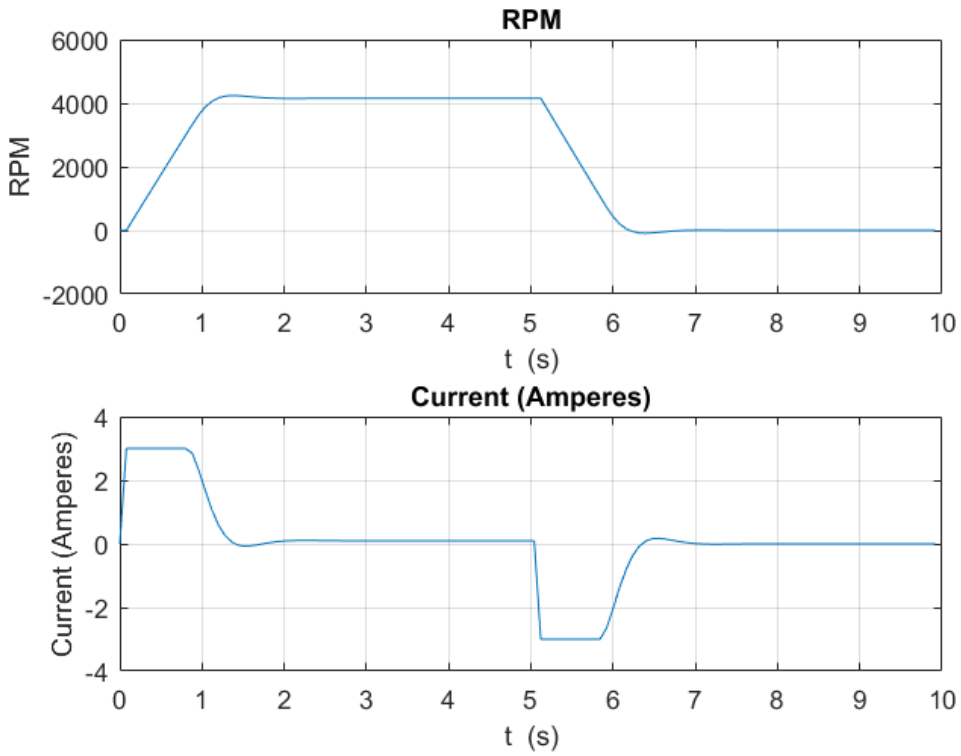

Figure 3.2 : Motor Model Simulation Output for RPM and Current for $V = 8\,Volts$

3.2 Modelling Reaction Wheel Actuated System

In order to test the RWs, a platform is needed. In some cases air bearing platform is used to test the behaviour of the reaction wheels in three axes.

In this case, a low cost solution is proposed. The platform will be able to rotate about two axes, pitch and yaw. It will be mounted on a base and rotating parts will be on bearings.

In the air bearing test case, it is nearly frictionless environment to test the RWs. However, with normal bearings, a friction model needs to be employed to increase the fidelity of the model.

For the inital tests, a readily available 2DOF Helicopter Test Platform seen in Fig. 3.3 is utilized. First the mathematical model given by the manufacturer is tested for the yaw motion with restricting it on the pitch axis. In the given mathematical model, only viscous friction is taken into account. The experiments on the platform showed that, in order to increase the fidelity of the model, a valid friction model needs to

be implemented. Before coming to this conclusion, here are the experiments and the system identification approach to obtain the physical parameters.

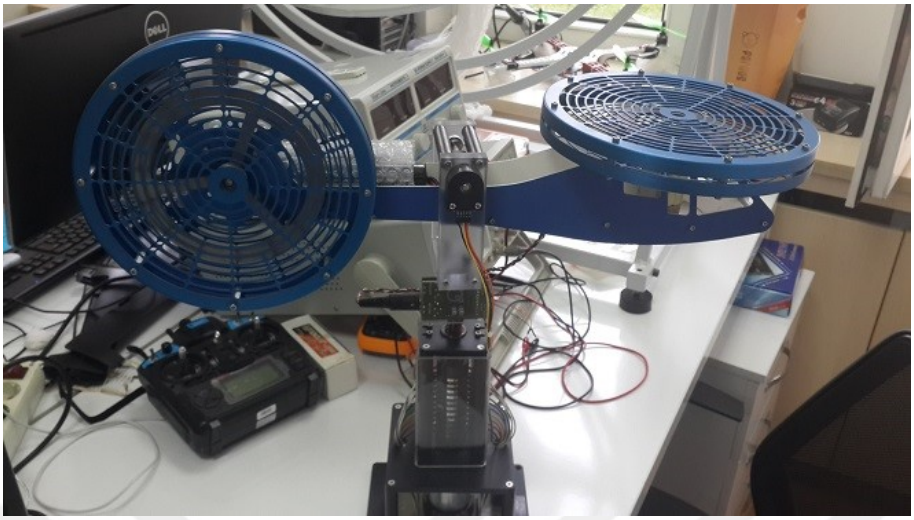

Figure 3.3 : 2DOF Reaction Wheel Test Platform

The equation of motion for yaw axis in helicopter configuration:

$$I\ddot{\psi} + b\dot{\psi} = K_{yy}V \tag{3.4}$$

In the experiment with the 2DOF Helicopter Test Mechanism, only the yaw motor is used, and yaw motion is studied in order to find a friction model. In the equation 3.4, even small amount of control moment can rotate the system. However, in the experiment, it is observed that, the voltages less than 4V cannot rotate the system. This gives rise to the error in the friction compensation. Thus a new friction model needs to be proposed. The parameters are described and their values are given in Table 3.2.

3.2.1 System Identification

The equation 3.4 is converted into Laplace domain.

Transfer function for the voltage input to the ψ angle output becomes:

$$\frac{\psi(s)}{V(s)} = \frac{\frac{K_{yy}}{I}}{s^2 + \frac{b}{I}s} \tag{3.5}$$

In order to identify the physical coefficients, the yaw motor is excited with a square wave voltage and several experiments are conducted on the platform. Here, given two experiment for the purpose of identifying the parameters.

Table 3.2 : Parametes of the 2DOF Platform.

Parameter	Explanation	Value	Unit
I	Total Inertia About Z Axis	2.28e-1	kgm^2
b	Friction Coefficient About Z Axis	0.082	Nms/rad
K_{yy}	Torque Constant	0.428	N/V

3.2.1.1 First Experiment

For the first experiment, -4Volts constant voltage and 0.4 Volt square wave voltage is applied. The transfer function given by System Identification Toolbox of MATLAB:

The transfer function given in Eq. 3.5 is named Model 2 in the simulation seen in Fig. 3.5.

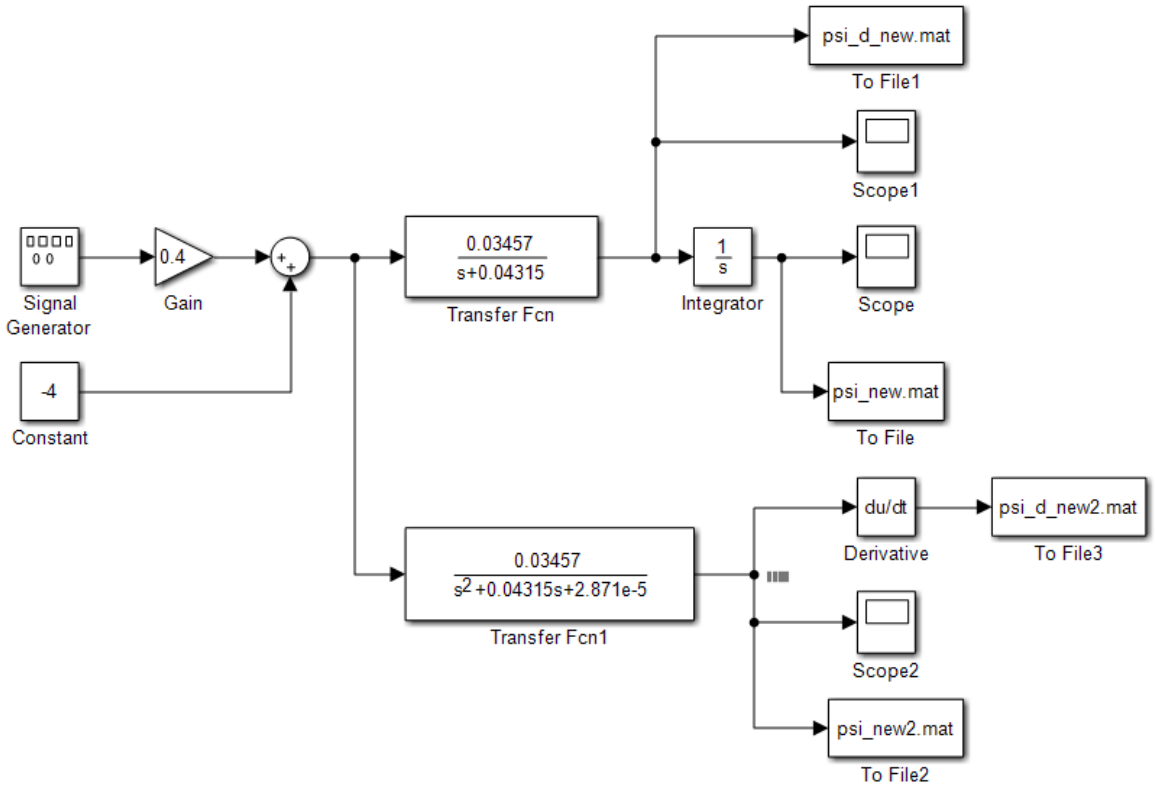

Figure 3.4 : MATLAB Simulink Diagram for Model Validation.

3.2.1.2 Second Experiment

For the second experiment, -5Volts constant voltage and 1 Volt square wave voltage with a frequency of 0.02 rad/s applied on the yaw motor. The transfer function given by System Identification Toolbox of MATLAB:

$$\frac{\psi(s)}{V(s)} = \frac{0.08911}{s+0.09091} \tag{3.6}$$

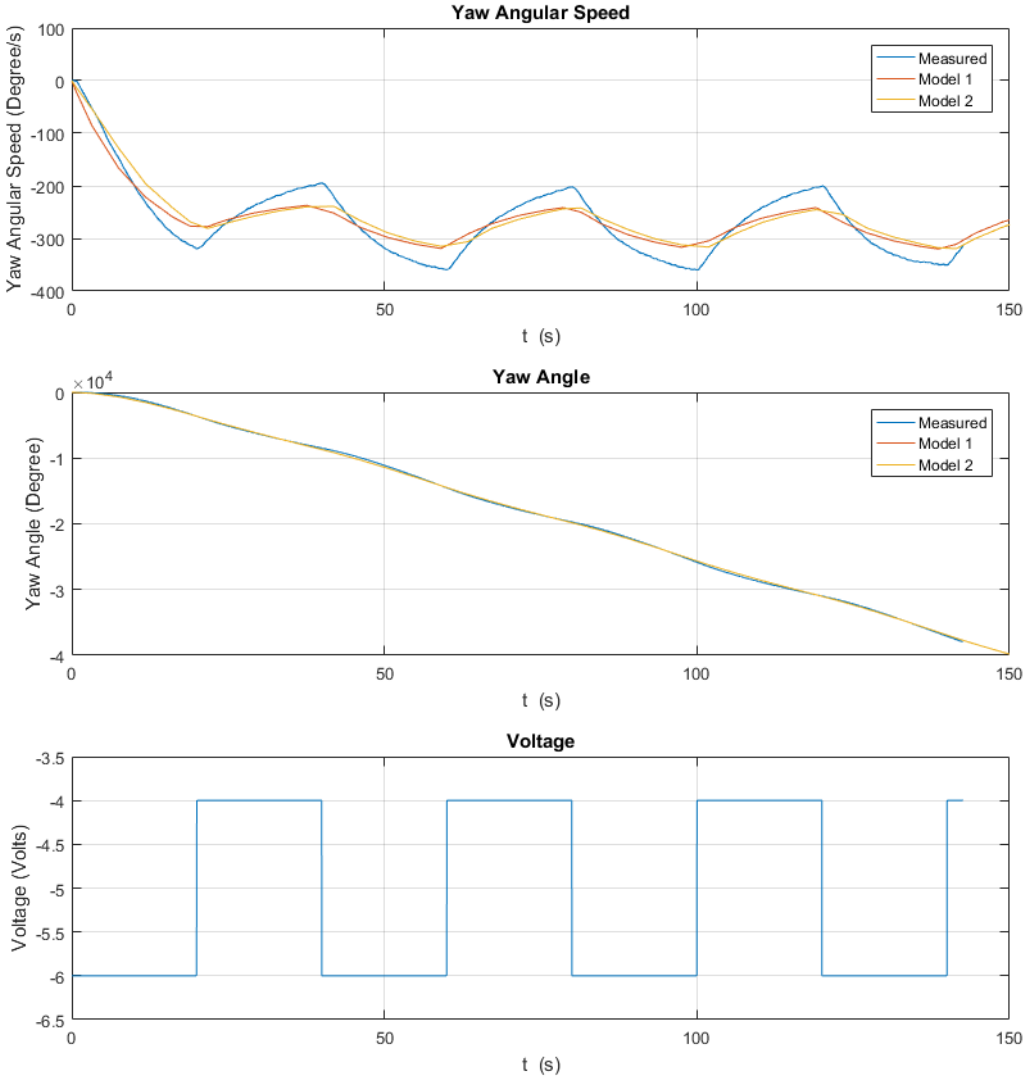

Figure 3.5 : System Identification Validation (First Experiment).

3.2.2 Friction Model

Several experiments and identification processes are conducted on the platform and two of them are presented in the previous section. In each experiment, a model is obtained with the given experimental data, the model output is compared with the measured values of the angle and angular speeds. It is observed that the models cannot overlap with the experimental data, for both angular speed and angle responses. It is also known that, in the mathematical model representing the system, even a small amount of control moment can rotate the system. However in the experiments, it is observed that the voltages below 4 Volts cannot rotate the system. This can be explained with static friction phenomena.

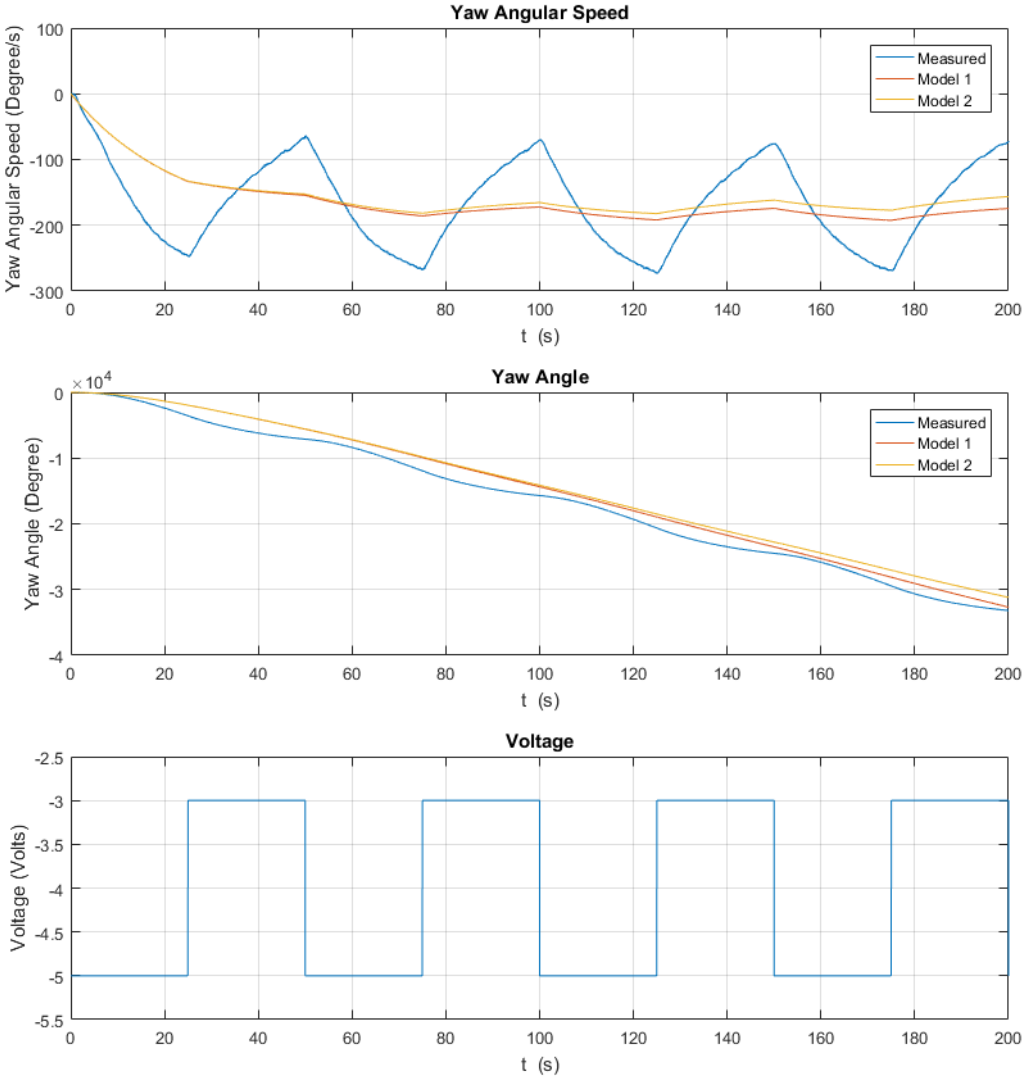

Figure 3.6 : System Identification Validation (Second Experiment)

In order to propose a better mathematical model, the literature on friction is surveyed.

3.2.2.1 The Coulomb Model

The classical way to model static friction is the Coulomb model. In the Coulomb friction model:

$$F_c = \mu F_n sign(v) \tag{3.7}$$

here F_n is the normal force, μ is the friction coefficient, v is the velocity of the object [17] [18]. This model is a candidate for the testbed friction behaviour.

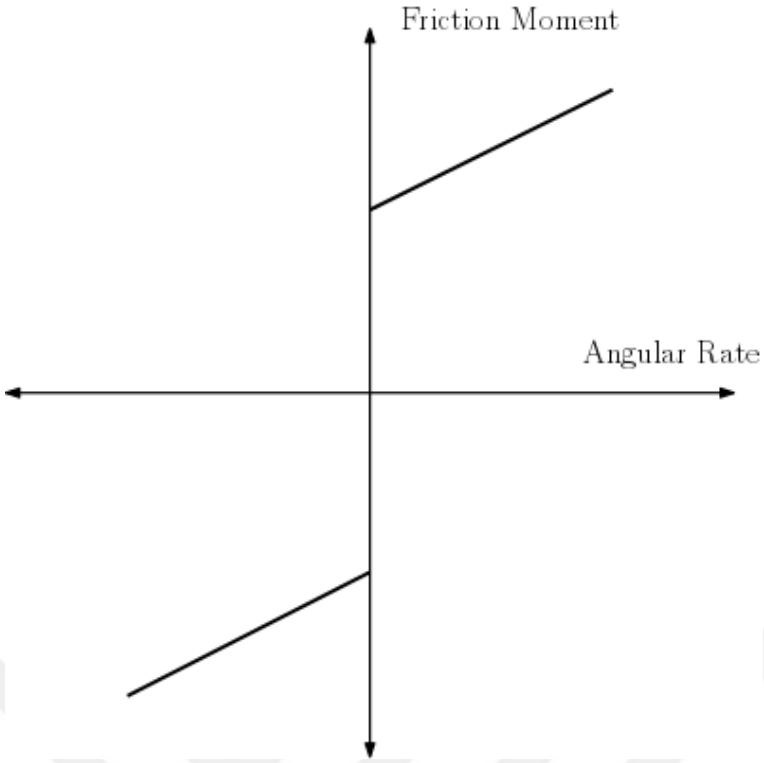

Figure 3.7 : Coulomb Friction Representation.

3.2.2.2 The Stribeck Model

In the coulomb friction model, after the static friction is overcome, the friction force/torque does change with the speed linearly. In the Stribeck Model, there are four phases, phase 1: no sliding which is where the static friction effect occurs, after the static friction is overcome there comes the second phase: boundary lubrication. In this phase, the friction force/moment remains the same. In the third phase, which is partial fluid lubrication, the friction force/moment decreases with increasing velocity. In the fourth and last phase, full fluid lubrication, the friction force/moment increases with increasing velocity [17] [18].

3.2.2.3 The Dahl Model

In the Dahl model, friction is described with an analogy of stress-strain behaviour of materials. Dahl assumed that the friction force is not only a function of velocity, but a function of displacement as well [17] [18].

The formulation:

$$\frac{dF_f(x)}{dx} = \sigma \left| 1 - \frac{F_f}{F_c} sign(\dot{x}) \right|^n sign\left(1 - \frac{F_f}{F_c} sign(\dot{x}) \right) \tag{3.8}$$

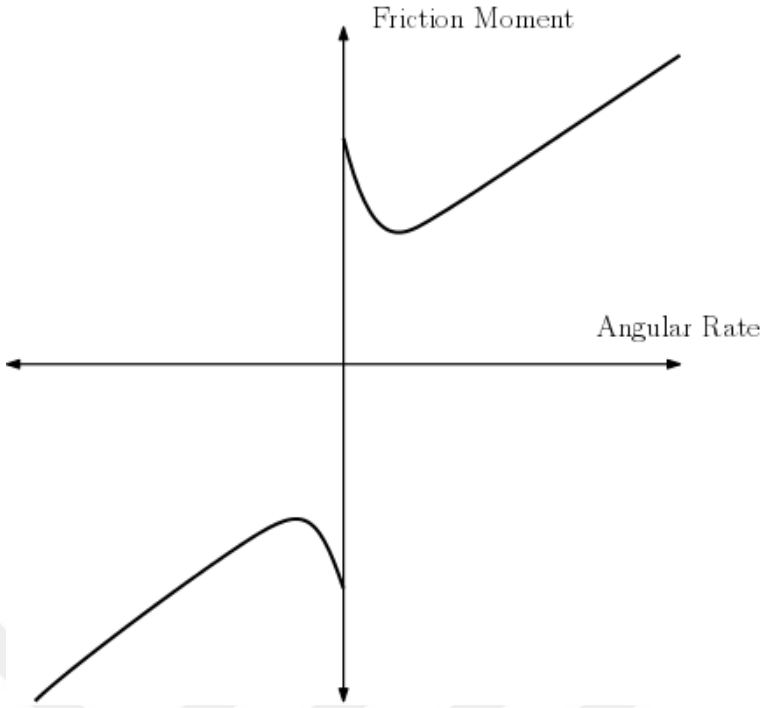

Figure 3.8 : Stribeck Friction Representation.

where σ is the stiffness parameter at equilibrium point $F_f = 0[N]$, F_c is Coulomb friction, n is a material dependent parameter, $0 \leq n \leq 1$ for brittle materials, $n \geq 1$ for more ductile materials [17] [18].

3.2.3 Identification of the Friction Model

In order to validate the model and determinde the friction model coefficents several experiments are done on the test platform seen in Fig. 3.3. Literature is surveyed to gain insight on the determination of the model parameters, and to choose the best suited model. After several trial and error process, it is decided that the Stribeck friction model best suits the behavior of the testbed.

A methodology is developed and applied to determine the model parameters, depending on the data recorded on the experiments. Friction cannot be directly measured, therefore from the measurement of the angle, angular rate; an experimental estimation of the friction is obtained.

In this process, the testbed is turned into a form that it can move only about the yaw axis, this makes it single input single output system.

The equation of the system can be written in such form:

$$I\ddot{\psi} + M_f = \tau(V) \tag{3.9}$$

where ψ is the yaw angle, I is the inertia about the yaw axis, M_f is the friction moment about the yaw axis, V is the voltage, $\tau(V)$ is the moment applied by the motor.

When the system has an initial velocity and there is no voltage on the motor, the equation of motion becomes:

$$\begin{aligned} I\ddot{\psi} + M_f &= 0 \\ I\ddot{\psi} + b_0\dot{\psi}^3 + b_1\dot{\psi}^2 + b_2\dot{\psi}^1 + b_3 &= 0 \end{aligned} \tag{3.10}$$

In order to capture the Stribeck curve, the friction is modelled as a third degree polynomial of the angular rate.

The equation can be rewritten as:

$$b_0\dot{\psi}^3 + b_1\dot{\psi}^2 + b_2\dot{\psi}^1 + b_3 = -I\ddot{\psi} \tag{3.11}$$

In the Eq. 3.11, $\dot{\psi}$ is a known quantity. The angle ψ is measured directly by the encoder, $\dot{\psi}$ is obtained by applying a derivative filter to the angle. The inertia I is also a known quantity. The friction related coefficients b_0, b_1,b_2, b_3 are unknown parameters and to be estimated. If $\ddot{\psi}$ is known, the friction related coefficients can be estimated by using the least squares method on the experimental data. However, applying a derivative filter to the angular rate $\dot{\psi}$ gives a noisy result and cannot be used. Another solution is to model the angular rate $\dot{\psi}$ as a function of time when there is no external torque applied on the system. If a function can be obtained, the time derivative of this function can be taken to obtain $\ddot{\psi}$.

In Fig. 3.9 the time response of the angular rate can be seen. The polynomic function is found using least squares method. This function is than derivated to get the $\ddot{\psi}$. Now, the only unknowns in the equation of motion are the b terms. They can be identified again by least squares regression.

The time dependent function (Eq. 3.12) of the angular rate $\dot{\psi}$ is obtained using least squares method with the help of experimental data.

$$\dot{\psi} = \left(6.7 \times 10^{-5}\right) t^4 + \left(-4.1 \times 10^{-3}\right) t^3 + \left(-9.5 \times 10^{-2}\right) t^2 + (-1.3)\, t + 10.9 \tag{3.12}$$

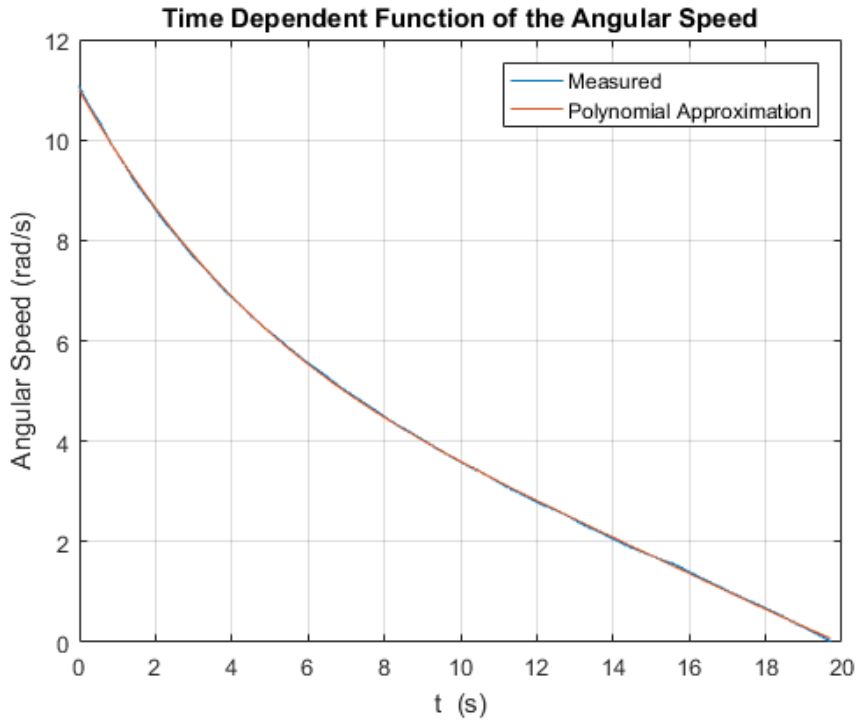

Figure 3.9 : Angular Rate as a Function of Time.

In order to estimate the friction coefficients seen in Eq. 3.11, the second derivative of the angle is needed. The time dependent function of the angular rate is derivated with respect to time, can be seen in Eq. 3.13

$$\ddot{\psi} = \left(2.68 \times 10^{-4}\right) t^3 + \left(-1.23 \times 10^{-2}\right) t^2 + \left(-1.9 \times 10^{-1}\right) t + (-1.3) \qquad (3.13)$$

The function relating angular rate and angular acceleration is estimated using least squares method with the experimental data. At each time step the measured angular rate is known, the estimated second derivative of the angle is also known quantity. Considering the equation of motion (Eq. 3.11) the relation between $\ddot{\psi}$ and $\dot{\psi}$ is obtained.

$$I\ddot{\psi} = \left(-6.89 \times 10^{-4}\right) \dot{\psi}^3 + \left(2.05 \times 10^{-2}\right) \dot{\psi}^2 + \left(-5.25 \times 10^{-1}\right) \dot{\psi} + (0.375) \quad (3.14)$$

In Fig. 3.10 the friction moment as a function of the angular rate can be seen. In the horizontal axis is the angular rate $\dot{\psi}$, in the vertical axis is the friction moment. The coefficients seen in Eq. 3.14 are b_0, b_1,b_2, b_3, respectively.

In the initial mathematical model, friction was modelled as viscous friction, however in the experiments, it was observed that for some voltages the system cannot be rotated.

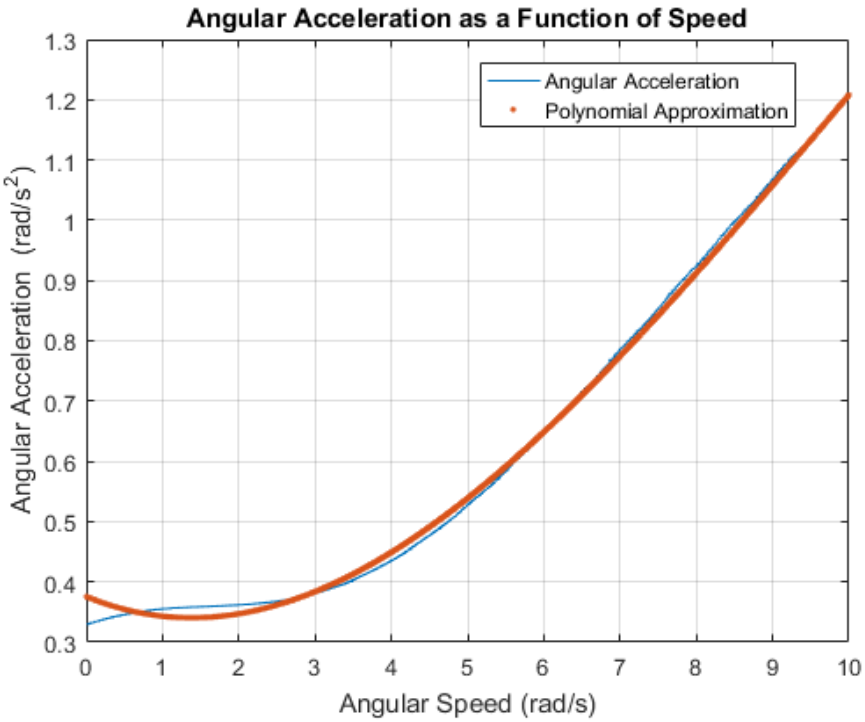

Figure 3.10 : Friction as a Function of Angular Rate.

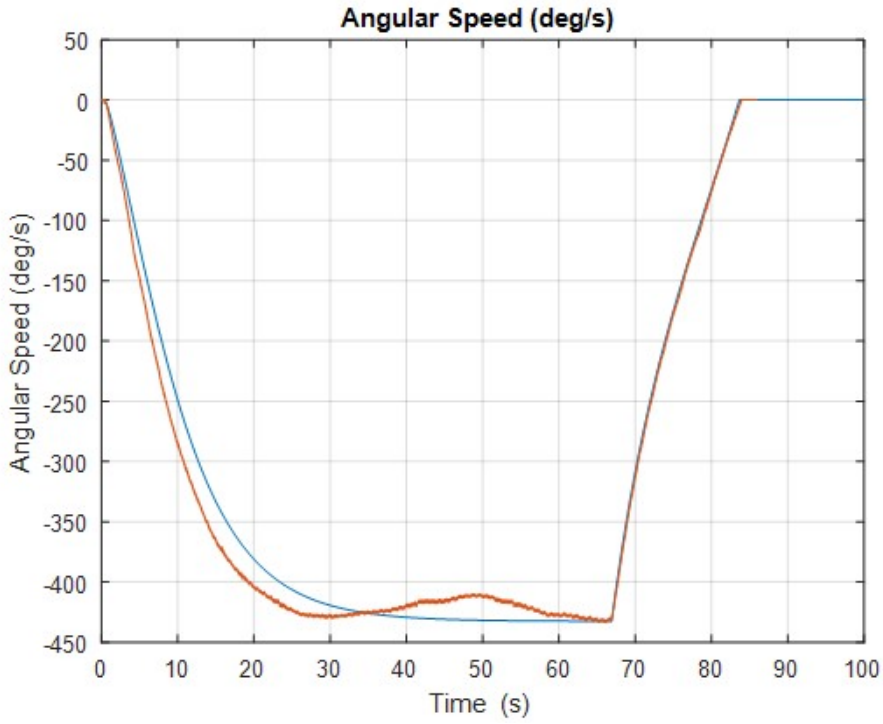

Figure 3.11 : Time Response of Angular Speed for the Applied Voltage of 6.7 Volts.

This phenomena is explained as static friction in the literature. In the scope of the thesis, a systematic method is employed to identify the friction model experimentally, a two stage least squares method is utilized. As a conclusion, the mathematical model with the identified parameters became a more reliable model comparing it to the inital

model. However, it should be noted that, this model is highly nonlinear and it has the switching property due to the friction model.

4. CONTROLLER DESIGN

In this chapter, two types of controllers are designed and applied on the simulations and on the real testbed. The first one is on-off controller, the second one is a parameter space approach based Proportional-Derivative (PD) controller.

4.1 On-Off Controller Design

In the section about RW design, it was found out how much time the spacecraft could scan according to the properties of the reaction wheel. Using the same mass and inertial properties, the equation of motion of the spacecraft is solved numerically, using only one reaction wheel and assuming it only rotates around an axis. The spacecraft will be controlled around the z-axis. The desired reference value will be reached with an on-off controller.

At this stage, the control signal required to perform a particular maneuver in a minimum time with a known reaction wheel of a known S/C of inertial properties is calculated as open loop and the resultant controller is applied on the computational simulation system and the results are presented. The open loop control signal is obtained by integrating the equations of motion at certain time intervals. The acceleration and deceleration characteristics of the reaction wheel are as in Fig 4.1. To scan the positive angle, the RT should be rotated in the negative direction, and the negative angle should be rotated in the positive direction to scan. In this example; a positive maneuver is desired. Starting angle and desired angle to be reached:

$$\theta_i = 0^\circ \qquad \theta_f = 90^\circ \tag{4.1}$$

The maneuver will be carried out in three stages. In the first phase, RW will be at zero speed, the maximum speed it can reach (4000 rpm). At the second stage, the RW will rotate at the limit speed and the spacecraft will have a certain angular velocity. After a certain angle is scanned, the RW will slow down and stop at the third stage. At the

moment the RW is stopped, the angular velocity of the spacecraft is zeroed and the desired orientation maneuver is performed. The equation of motion:

$$I_{SC}\ddot{\theta} + J\dot{\Omega} = 0 \tag{4.2}$$

Here, the total moment of inertia of the I_{SC} spacecraft is the moment of inertia of the J reaction wheel, while the $\dot{\Omega}$ is the acceleration of the RW, which is also equal to the slope of the graph in Fig. 4.1 in the first and third regions. In this example, acceleration and deceleration are thought to be linear and equivalent. In the equation of motion, I_{SC}, J and Ω, $\dot{\Omega}$ at $t = 0$ are known, the initial value problem can be solved. Since the acceleration behavior of RW is known, the time to reach the maximum speed of RW can be calculated. If the equation of motion is integrated in this time period, the rotation angle at t_1 is:

$$\theta_{t_1} = -\frac{J}{I_{SC}}\dot{\Omega}\frac{t_1^2}{2} = \theta_{t_3} \tag{4.3}$$

Since the same amount of angle will be scanned at the deceleration time, the equation $t_1 = t_3$ is valid. If $t_1 + t_3$ is removed, the angle to be scanned in the second stage can be found. The time spent in the second stage can be calculated from this.

$$\theta_{t_2} = \theta_f - (\theta_{t_1} + \theta_{t_3}) \tag{4.4}$$

The equation of motion in the second phase:

$$I_{SC}\ddot{\theta} = 0 \tag{4.5}$$

If it is solved for the duration of t_2

$$\theta_{t_2} = \dot{\theta}_{t_1} t_2 \tag{4.6}$$

The angle θ_{t_2} that is covered in time t_2 is calculated earlier, the time in the second phase can be calculated. This time is important because when to slow down the wheel should be known.

In Fig. 4.2, the simulation result shows the orientation angle and angular velocity graphs of the spacecraft. In the first region, the angular velocity increased and in the

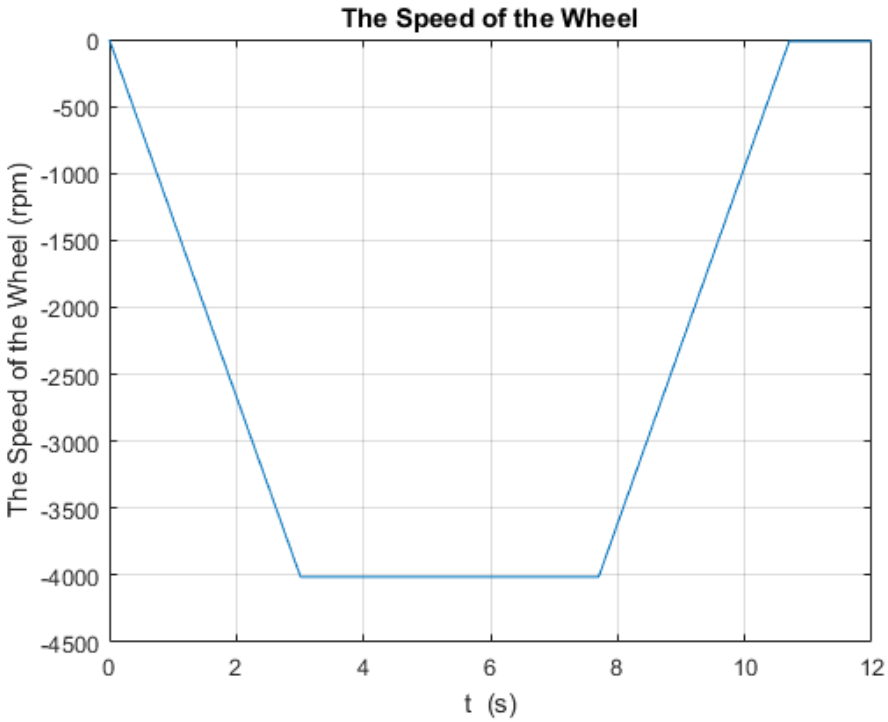

Figure 4.1 : RW Speed Time Response

second stage the speed of the reaction wheel was constant as the speed of the reaction wheel was fixed. In the third zone, due to the wheel being decelerated, an acceleration in the opposite direction has occurred and the speed of the vehicle has become zero when the desired angle has been reached.

As can be seen from the orientation angle graph, after $t_1 + t_2 + t_3$ period, the vehicle performed the desired steering maneuver and no deviation was observed. This method was made assuming that there were no disturbing effects for the minimum time maneuver. However, in a real scenario, there may be effects that will cause the system and RW to behave differently than expected.

4.2 Linear Controller Design Based on Parameter Space Approach

In order to design a linear controller for this system, model is represented in Laplace domain. The equation of motion about Z axis:

$$I\ddot{\psi} + \left[b_0\dot{\psi}^3 + b_1\dot{\psi}^2 + b_2\dot{\psi} + b_3\right] sgn\left(\dot{\psi}\right) = \tau_z \tag{4.7}$$

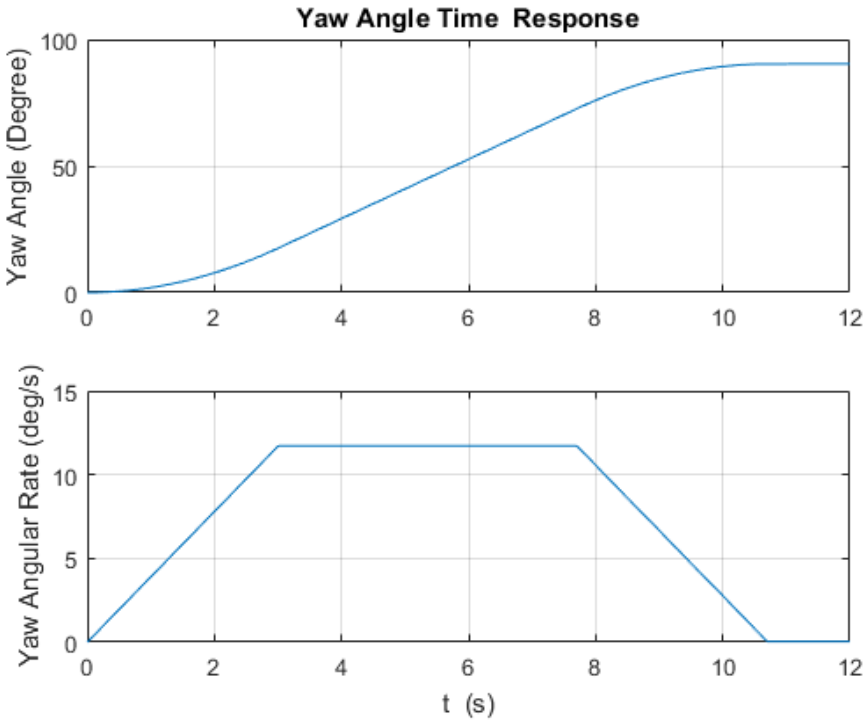

Figure 4.2 : S/C Angle and Angular Speed Time Response for On-Off Control

If the angle to be rotated and the angular speed is assumed to be small, and the static friction to be compensated with a feedforward term. The equation of motion can be simplified to this form:

$$I\ddot{\psi} + b_2\dot{\psi} = \tau_z \tag{4.8}$$

The Laplace domain representation:

$$\frac{\Psi(s)}{T_z(s)} = \frac{\frac{1}{I}}{s\left(s + \frac{b_2}{I}\right)} \tag{4.9}$$

The motor equations are transform into Laplace domain as voltage is the input and angular speed of the wheel is the output.

$$\frac{\Omega(s)}{V(s)} = \frac{K}{[(Js+b)(Ls+R)+K^2]} \tag{4.10}$$

Finally the motor, wheel and the rotational system about Z axis can be represented as one transfer function: voltage as the input and the angle about Z axis ψ is the output. The parameters in Eq. 4.12 are listed in Table 3.1

$$\frac{\psi(s)}{V(s)} = \frac{\frac{JK}{I}s}{[(Js+b)(Ls+R)+K^2]\left[s\left(s + \frac{b_2}{I}\right)\right]} \tag{4.11}$$

Controller design for this simplified form can be implemented and furthermore, stability analysis can be performed.

The controller is in the Proportional-Derivative form:

$$G(s) = K_p + K_d s \tag{4.12}$$

Controller design is implemented based on the method described in [19].

The controller is designed to be a PD based controller. K_p and K_d are taken as uncertain parameters in the transfer function and the stability region in $K_p - K_d$ plane is searched.

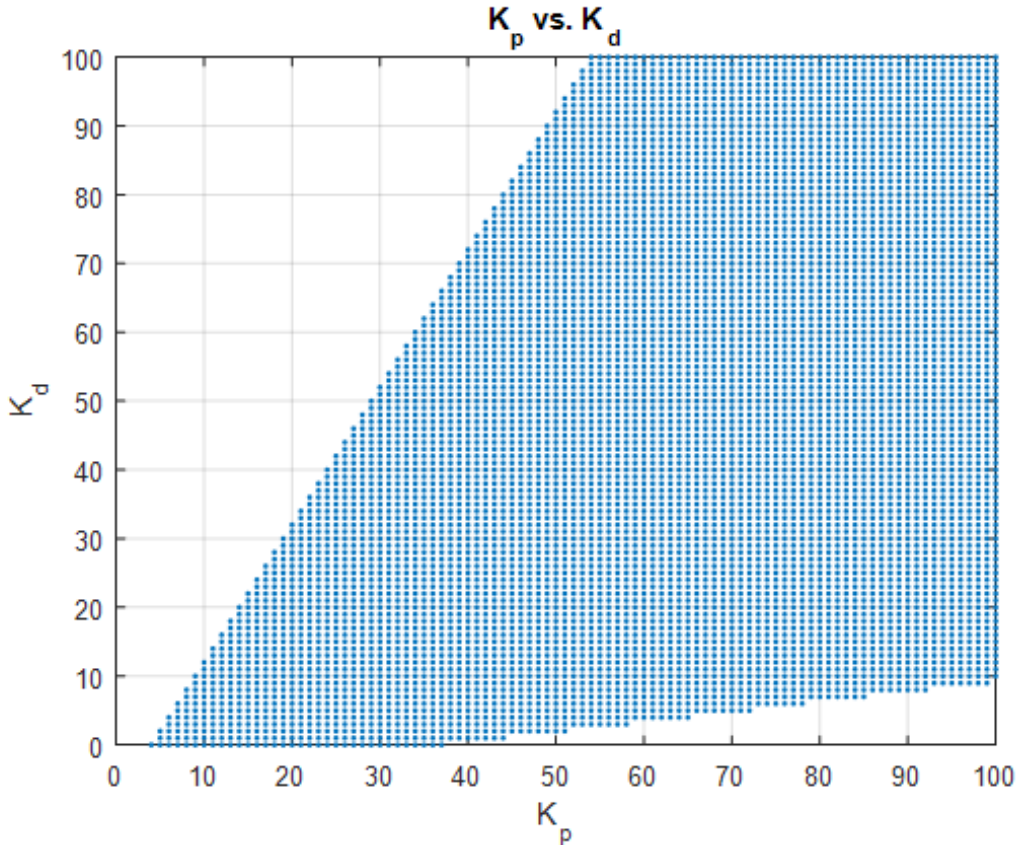

Figure 4.3 : Stability Region in $K_p - K_d$ plane

The simulations are run for several reference inputs, and K_p, K_d combinations, the results are listed in Figs. 4.5, 4.6, 4.7, 4.8, 4.9, 4.10, 4.11.

In the process of controller parameter tuning, K_p - K_d pairs are chosen from the stability region seen in Fig. 4.3. Several options are tested on simulation environment first and then on the real test platform.

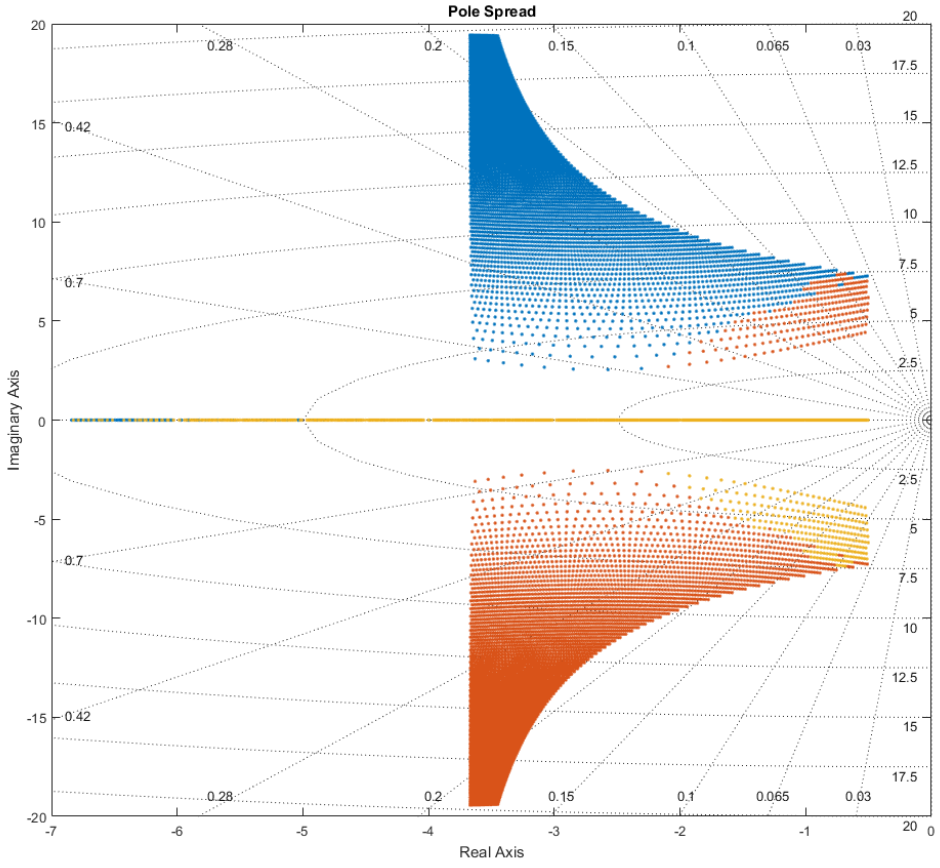

Figure 4.4 : Pole Spread for the Stable K_p - K_d pairs seen in Fig. 4.3

In Fig. 4.5, 4.6, the reference signal to be tracked is a 10 degrees square wave. The controller is driving the system near to the reference, however there is a steady state error.

In Fig. 4.7, several K_p - K_d are tested on the system for 10 degrees square wave reference signal. It can be observed that, as the controller gain for K_p increases, the reference tracking performance gets better. For the case of $K_p = 100$, $K_d = 10$ the steady state error is minimal. It is also observed that as the K_p is increased more, the control signal increases and saturation occurs.

The first part of the tests are done for the same reference signal. For the next case, the reference signal is changed and the controller parameter is fixed at $K_p = 100$, $K_d = 10$. In Fig. 4.9 the time response can be observed for 20 degrees of square wave reference signal.

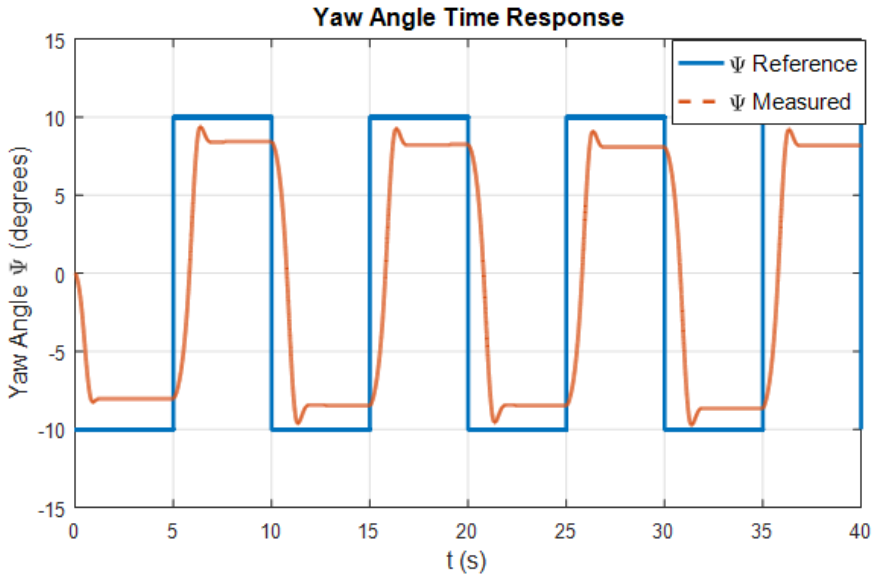

Figure 4.5 : Yaw Angle Time Response $K_p = 40$ and $K_d = 10$

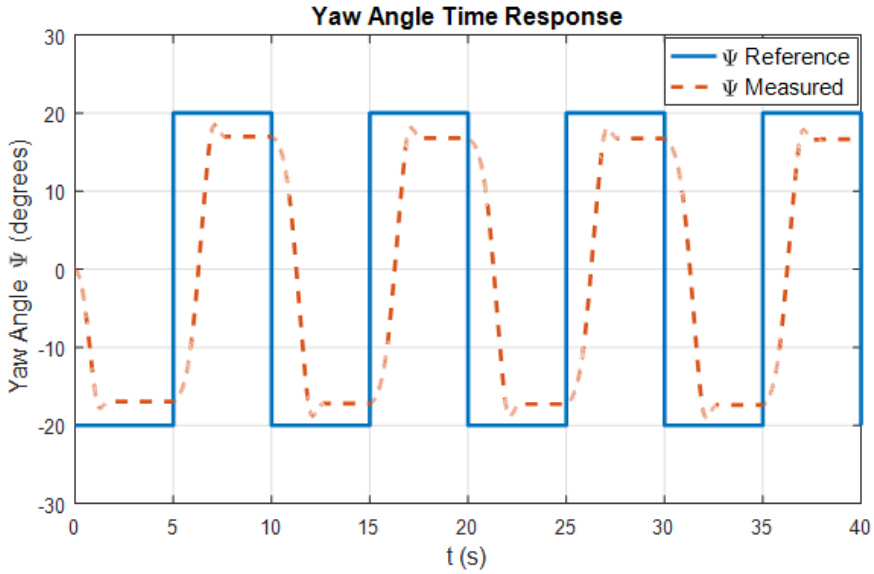

Figure 4.6 : Yaw Angle Time Response $K_p = 40$ and $K_d = 10$

In Figs. 4.9, 4.10 and 4.11 the overshoot effect increases as the reference angle gets bigger. This is due to the high gain, high error combination. However the reference tracking performance of the controller is not decreased.

It can be seen that the time response of the angle has a steady state error, considering all the figures. This should be minimized or diminished by modifying the controller with an integral component. If it were possible to rotate the wheels without a limit speed, this would be a solution. For future work, the excess momentum can be dumped to the static friction torque by slowing down the flywheels in a controlled fashion.

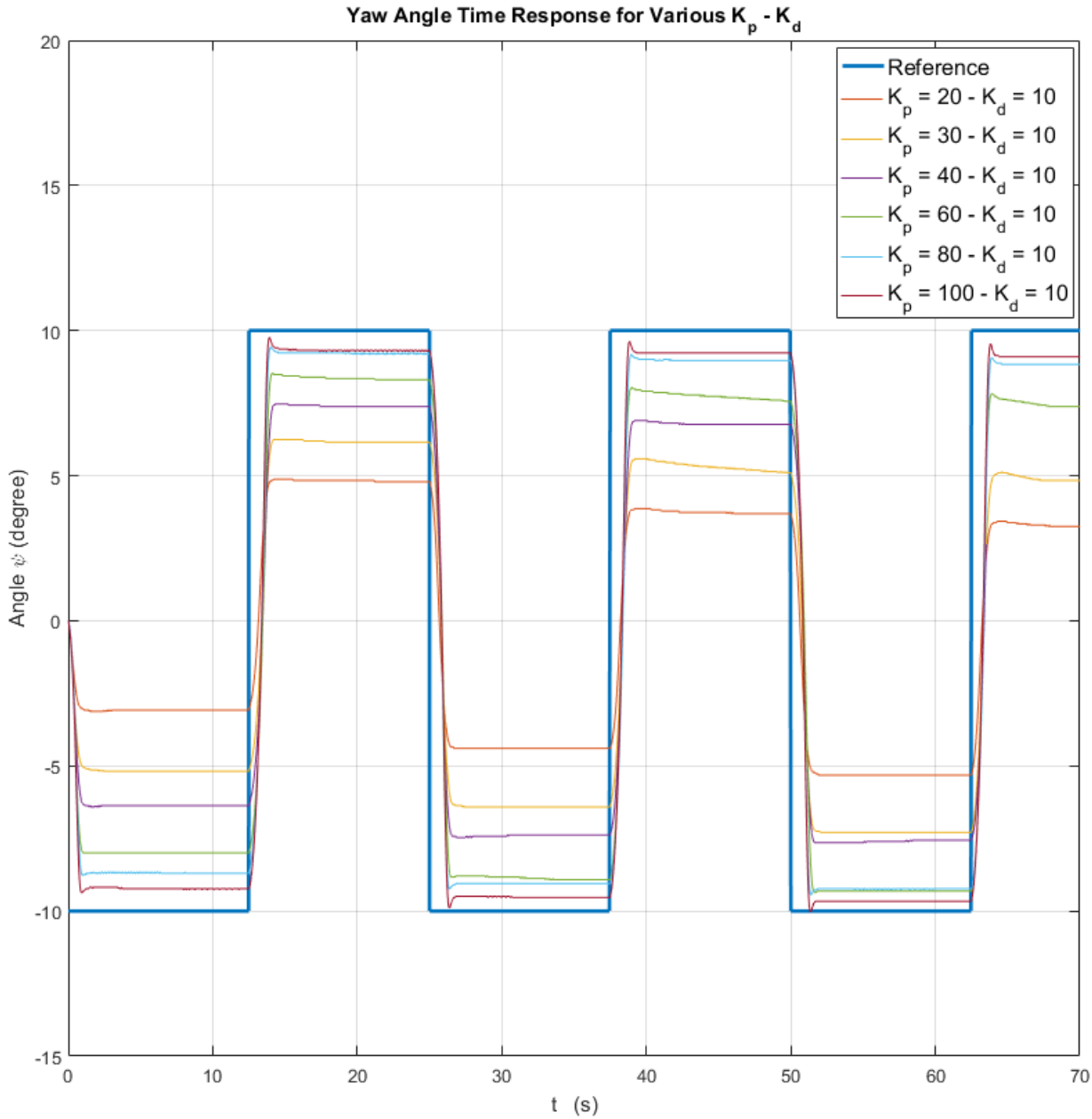

Figure 4.7 : Yaw Angle Time Response for Various K_p - K_d

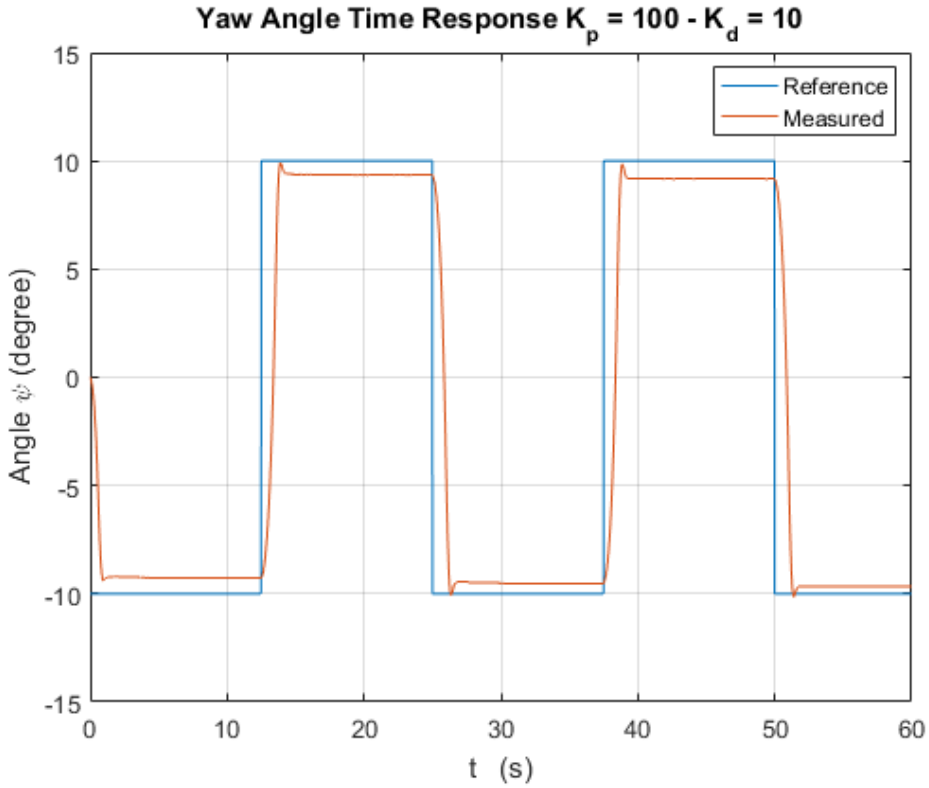

Figure 4.8 : Yaw Angle Time Response for $K_p = 100$ and $K_d = 10$, Reference 10 Degree Square Wave

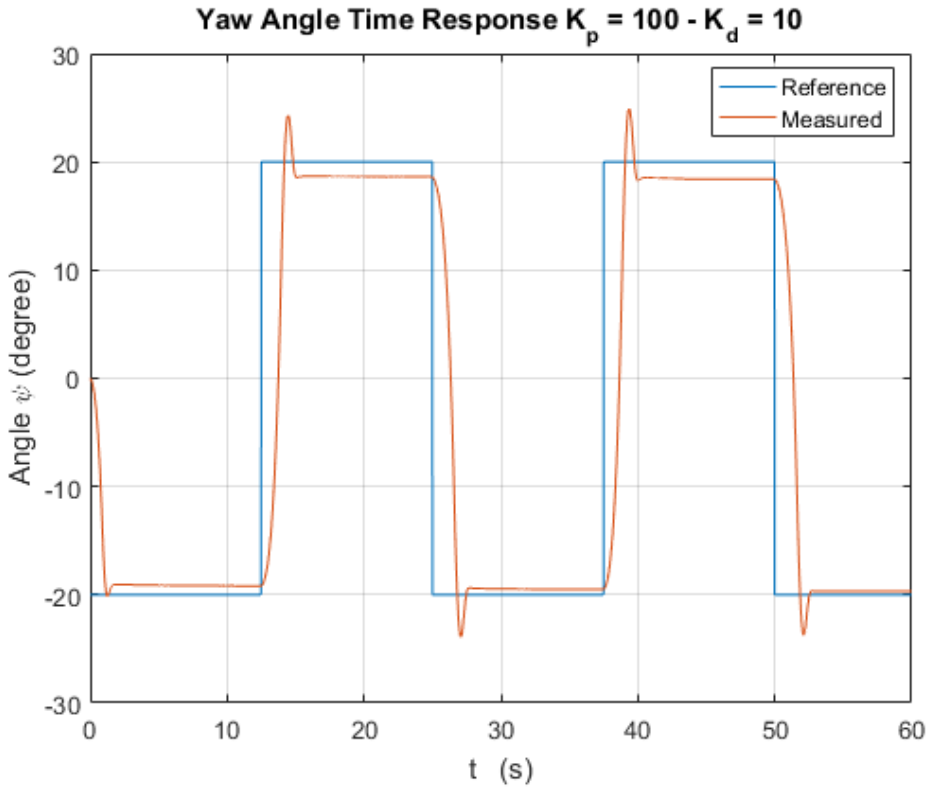

Figure 4.9 : Yaw Angle Time Response for $K_p = 100$ and $K_d = 10$, Reference 20 Degree Square Wave

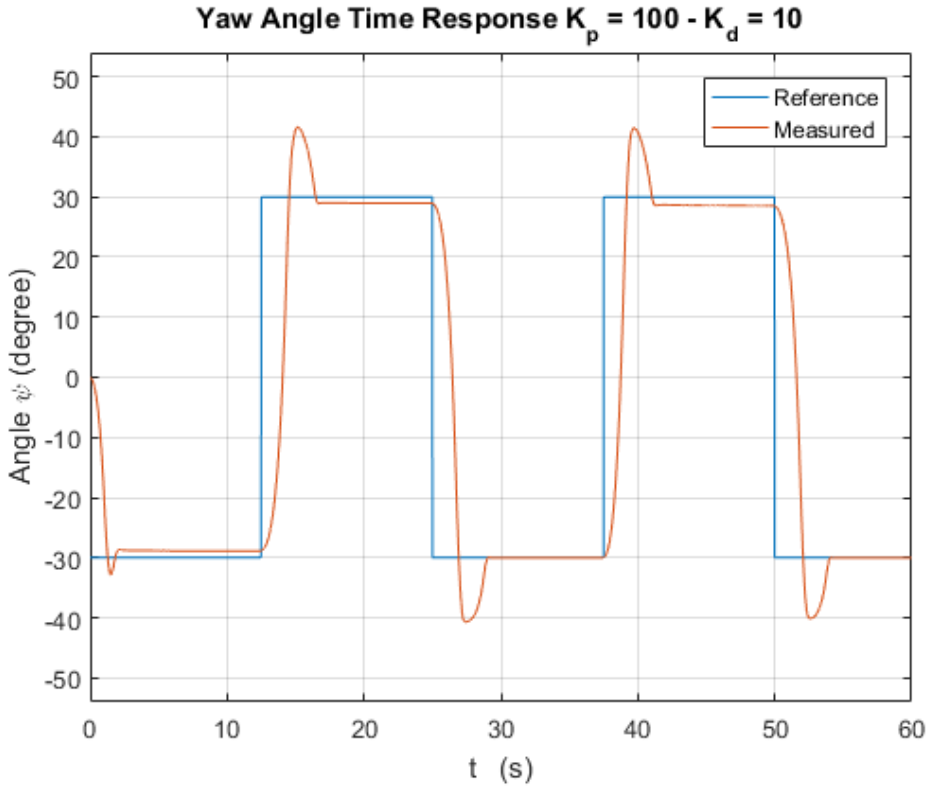

Figure 4.10 : Yaw Angle Time Response for $K_p = 100$ and $K_d = 10$, Reference 30 Degree Square Wave

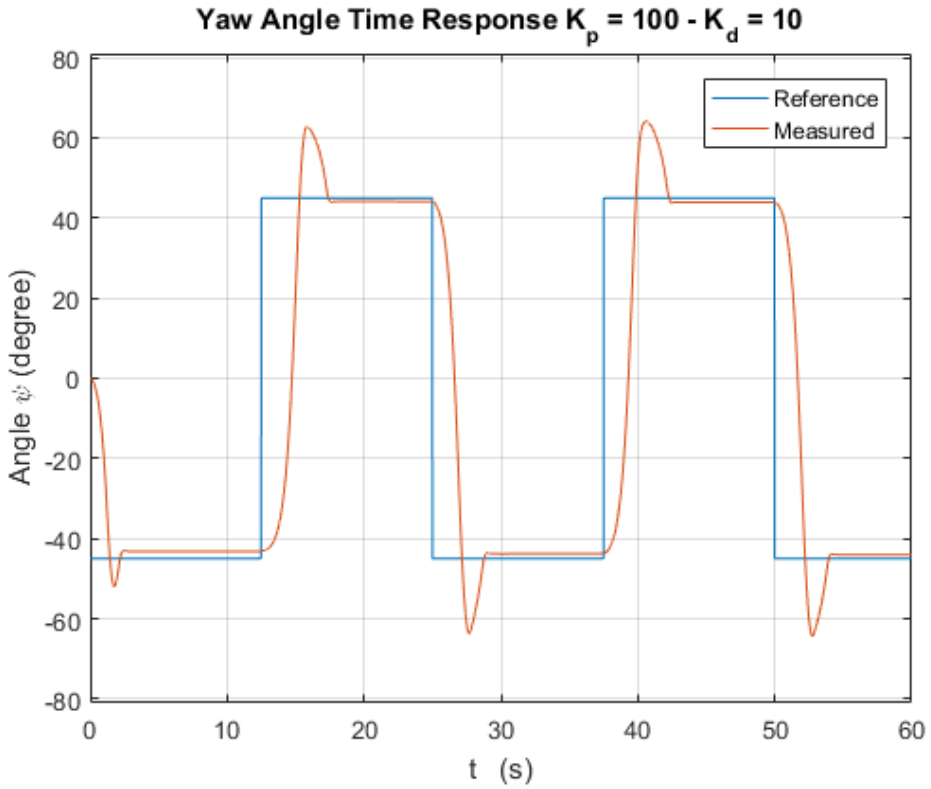

Figure 4.11 : Yaw Angle Time Response for $K_p = 100$ and $K_d = 10$, Reference 45 Degree Square Wave

5. CONCLUSIONS AND RECOMMENDATIONS

In this thesis, a RW and a RW actuated testbed design, modelling and controller design is taken as a research subject. RW is a dynamical system, it is used in space applications to actively control the orientation of the S/C. The purpose of the thesis was to design a platform to be able to identify the system initially, to obtain a high fidelity model and to validate it with experimental data. The final objective of the thesis is to be able to test control methods on RW actuated system.

In the first stage of the thesis, the literature survey is conducted on RW systems. It is observed that practical test environment is needed to be able to do realistic tests on control actuators. Test environments such as air bearing platforms and gyroscopic platforms are researched. It is decided to design and manufacture a two degree of freedom test platform to test the reaction wheels. The reaction wheels are designed according to the maximum inertia of the possible testbed. There have been multiple designs in this process and finally RW and test platform are manufactured.

In the second stage, reaction wheel and the testbed is modelled mathematically with the laws of physics. Initially, it is observed that the model output and the measurements does not match. The reason behind that is thought to be the friction model. In the mathematical model of the testbed, the friction representation did not include the static friction effect. The model is updated with the Stribeck friction model and its parameters are identified based on the method described in the thesis. Thus a high fidelity model is obtained to simulate the output of the designed controllers.

The last stage was to design and test controllers. A simplified version of the mathematical model is utilized based on assumptions to design a controller using parameter space approach. A plane of all possible PD controllers is obtained, several K_p, K_d combinations are chosen from this plane and tested on the platform. It is observed that increasing K_p helped the system to reach the desired angle quickly, with a possible cost of overshooting. It should be noted that the tests show PD based controller cannot overcome the steady state error. In order to close the gap, an integral

part could have been included to the controller. However this also comes with a cost, since the wheels have a saturation speed. In the S/Cs the excess momentum is dumped with other actuators. In this testbed, the excess momentum can be dumped to the static friction on the bearing, by slowing down the wheel in a controlled way.

For future applications, it is planned to manufacture four more RWs and a 3DOF test platform to be tested on gyroscopic test mechanism [2] in Model Lab. ITU. This research can be helpful understanding nonlinear systems' behaviour, friction phenomena and how to model and compensate it, to test controllers, to gain insight on the behaviour of RWs on S/Cs.

REFERENCES

[1] **Leve, F.A.**, **Hamilton, B.J. and Peck, M.A.** (2015). *Spacecraft momentum control systems*.

[2] **Hancer, M.**, **Bitirgen, R. and Bayezit, I.** (2018). Designing 3-DOF Hardware-In-The-Loop Test Platform Controlling Multirotor Vehicles, *IFAC-PapersOnLine*, *51*(4), 119 – 124, http://www.sciencedirect.com/science/article/pii/S2405896318303549, 3rd IFAC Conference on Advances in Proportional-Integral-Derivative Control PID 2018.

[3] **Carrara, V. and Kuga, H.K.** (2013). Torque and Speed Control Loops Of A Reaction Wheel, *11th International Conference on Vibration Problems*, (September), 9–12.

[4] **Wang, H.**, **Zhao, G. and Huang, H.** (2015). Minimum-Time Eigenaxis Rotation Maneuvers for a Spacecraft With Three Axis Reaction Wheels, *Journal of Dynamic Systems, Measurement, and Control*, *137*(11), 111004, http://dynamicsystems.asmedigitalcollection.asme.org/article.aspx?doi=10.1115/1.4030912.

[5] **Xinsheng, G.**, **Qizhi, Z. and Li-Qun, C.** (2006). Optimal motion planning for a rigid spacecraft with two momentum wheels using Quasi-Newton method, *Acta Mechanica Solida Sinica*, *19*(4), 334–340, http://dx.doi.org/10.1007/s10338-006-0640-6.

[6] **Jia, Y.H. and Xu, S.J.** (2005). Spacecraft attitude tracking and energy storage using flywheels, *Chinese Journal of Aeronautics*, *18*(1), 1–7, http://dx.doi.org/10.1016/S1000-9361(11)60274-4.

[7] **Hall, C.** (1997). High speed flywheels for integrated energy storage and attitude control, *Proceedings of the 1997 American Control Conference (Cat. No.97CH36041)*, *3*(June), 1894–1898.

[8] **Jia, Y.H.**, **Xu, S.J. and Tang, L.** (2004). Bias momentum attitude control system using energy/momentum wheels, *Chinese Journal of Aeronautics*, *17*(4), 193–199.

[9] **Ismail, Z. and Varatharajoo, R.** (2010). A study of reaction wheel configurations for a 3-axis satellite attitude control, *Advances in Space Research*, *45*(6), 750–759, http://dx.doi.org/10.1016/j.asr.2009.11.004.

[10] **Yoon, H.**, **Seo, H.H. and Choi, H.T.** (2014). Optimal uses of reaction wheels in the pyramid configuration using a new minimum infinity-norm solution,

Aerospace Science and Technology, *39*, 109–119, http://dx.doi.org/10.1016/j.ast.2014.09.002.

[11] **Shankar Narayan, S.**, **Nair, P.S. and Ghosal, A.** (2008). Dynamic interaction of rotating momentum wheels with spacecraft elements, *Journal of Sound and Vibration*, *315*(4-5), 970–984.

[12] **Middleton, D.B.** Angular Momentum From a Spacecraft Momentum-Exchange Gravity-Gradient Moments.

[13] **Spong, M.W.**, **Corke, P. and Lozano, R.** (2001). Nonlinear control of the Reaction Wheel Pendulum, *Automatica*, *37*(11), 1845–1851.

[14] **Brown, T.S.** (2016). The Cassini Reaction Wheels: Drag and Spin-Rate Trends from an Aging Interplanetary Spacecraft at Saturn, *AIAA Guidance, Navigation, and Control Conference*, http://arc.aiaa.org/doi/10.2514/6.2016-2085.

[15] **Gajamohan, M.**, **Merz, M.**, **Thommen, I. and D'Andrea, R.** (2012). The Cubli: A cube that can jump up and balance, *IEEE International Conference on Intelligent Robots and Systems*, 3722–3727.

[16] **Oland, E. and Schlanbusch, R.** (2009). Reaction wheel design for CubeSats, *RAST 2009 - Proceedings of 4th International Conference on Recent Advances Space Technologies*, (November), 778–783, arXiv:1011.1669v3.

[17] **van Geffen, V.**, A study of friction models and friction compensation.

[18] **Chou, D.** Dahl Friction Modelling.

[19] **Bitirgen, R.**, **Hancer, M. and Bayezit, I.** (2018). All Stabilizing State Feedback Controller for Inverted Pendulum Mechanism, *IFAC-PapersOnLine*, *51*(4), 346 – 351, http://www.sciencedirect.com/science/article/pii/S2405896318303859, 3rd IFAC Conference on Advances in Proportional-Integral-Derivative Control PID 2018.

APPENDICES

APPENDIX A : Codes
APPENDIX A.1 : Rotary Encoder Readings.
APPENDIX A.2 : The Code to Run the Designed RW Actuated System.
APPENDIX A.3 : Motor Model Simulation.
APPENDIX A.4 : Controller Design.

APPENDIX B : Figures of the Reaction Wheel and RW Actuated System
APPENDIX B.1 : RW Actuated System Designs

APPENDIX A.1: Rotary Encoder Readings.

```
/*
 *    Rotary Encoder Angle Readings
 */

#include <Servo.h>

// constants
#define POSMIN              -512
#define POSMAX              512
#define PWMMIN              1000
#define PWMMAX              1900

// pins
#define PINA                3
#define PINB                6

// rotary encoder position
volatile float pos;
volatile float pos_d, pos_d_new;
volatile float alpha;

float pos_prev, pos_new;
float t_new, t_prev;

// esc related variables
Servo   esc;
int             pwm;

void setup() {

        // pins
        pinMode(PINA, INPUT);
        pinMode(PINB, INPUT);
        //esc.attach(ESCPIN);

        // initialization(s)
        pos = 0;
        pos_d = 0;
        alpha = 0.95;
        pos_prev = 0;
        t_prev = 0;
        // interrupt for pos update
        attachInterrupt(digitalPinToInterrupt(PINA), checkPos);
```

```
        Serial.begin (9600);
}

void loop() {
        t_new = millis();
        pos_new = pos;
        // only the prints for the serial plotter

        Serial.print(2000);
        Serial.print("␣");
        Serial.print(PWMMAX);
        Serial.print("␣");
        Serial.print(PWMMIN);
        Serial.print("␣");
        Serial.print(POSMAX);
        Serial.print("␣");
        Serial.print(POSMIN);
        Serial.print("␣");

        if( isnan(pos_d_new) )
                pos_d = 0;
        else
                pos_d = pos_d*alpha + pos_d_new*( 1 - alpha );
        Serial.print(pos*360/205);
        Serial.println("␣");
        Serial.println(pwm);

        t_prev = t_new;
        pos_prev = pos_new;
}


void checkPos(){
        // called when PINA (of rotary encoder) changes
        // updates pos

        if(digitalRead(PINA) != digitalRead(PINB)) {
                pos += 0.1;
        }
        else {
                pos -= 0.1;
        }

        pos = constrain(pos, POSMIN, POSMAX);

}
```

APPENDIX A.2: The Code to Run the Designed RW Actuated System.

```
/*
 *       How to use:
 *       Do the pwm calculations in ISR() function.
 *       Fill RES1 and RES2.
 *
 *
 */
#include <SPI.h>
#include <SD.h>
#include <Servo.h>

#define TWO_PI 6.28318530717958647692528676655900

// pins
#define PINA1_          2
#define PINA2_          3
#define PINB1_          5
#define PINB2_          6

#define esc_1_pin       7
#define esc_2_pin       8

// consts
const int PWM_MIN       = 1100;
const int PWM_MAX       = 1800;

const int RES1  = 1024;
const int RES2  = 1024;


// vars
Servo esc_1;
Servo esc_2;

int pwm_1;
int pwm_2;
float tt;

// rotary encoder positions
volatile int    pos1;
volatile int    pos2;

volatile int    pos1_prev;
volatile int    pos2_prev;

volatile double speed1;
```

```
volatile double speed2;

// logging
File     log_file;
String   log_data;

void setup() {

        /* ESC */
        esc_1.attach(esc_1_pin);
        esc_2.attach(esc_2_pin);

        /* Rotary Encoder */
        pinMode(PINA1_, INPUT);
        pinMode(PINB1_, INPUT);
        pinMode(PINA2_, INPUT);
        pinMode(PINB2_, INPUT);

    pos1                = 0;
    pos2                = 0;
    pos1_prev    = 0;
    pos2_prev    = 0;

    attachInterrupt(digitalPinToInterrupt(PINA1_), checkPos1 );
    attachInterrupt(digitalPinToInterrupt(PINA2_), checkPos2 );


        /* Timer Interrupt */
        cli();

        // cleaning
        TCCR0A   = 0;
        TCCR0B   = 0;
        TCNT0    = 0;

        // CTC
        TCCR0A |= (1 << WGM01);
        // prescaler
        TCCR0B |= (1 << CS00) | (1 << CS02);
        // compare reg
        OCR0A = 0x9C;

        // enable
        TIMSK0 |= (1 << OCIE0A);

        sei();

        /* Logging */
```

```
        pinMode(SS, OUTPUT);

        Serial.begin(9600);
        // wait for serial
        while(!Serial) {};

        Serial.print("[Message] Initializing SD card.");
        if (!SD.begin(SS)) {
                Serial.println("[Error] Initialization failed!");
                while(true) {};
        }
        Serial.print("[Message] Initializing completed.");

        Serial.print("[Message] Oppening log file.");
        log_file = SD.open("log11.txt", FILE_WRITE);
        if(!log_file) {
                Serial.print("[Error] Couldn't open log file.");
                while(true) {};
        }
        Serial.print("Log file successfully opened.");
        log_file.println("pos1; pos2; pwm_1; pwm_2");
        log_file.println( micros() );
        log_file.close();  //!!!
        log_data = "";
        tt = 0;
}



void loop() {
        tt += abs( micros() );
        log_file.println(log_data);
        Serial.println(log_data);
        if ( tt > 300000 ) {
                log_file.close();
                Serial.println( "File Closed" ); }      //!!!
        Serial.println( tt );
        log_data = "";
}

ISR(TIMER0_COMPA_vect) {

        // default pwm
        pwm_1 = 1100;
        pwm_2 = 1100;

        // speed calculation (in rad/sec)
        speed1  = (((pos1-pos1_prev)/(RES1*2))/TWO_PI)/(0.01);
```

```
        speed2  = (((pos2-pos2_prev)/(RES1*2))/TWO_PI)/(0.01);

        pos1_prev       = pos1;
        pos2_prev       = pos2;

        // TODO: calculate pwm_1 and pwm_2 here

        // constrain PWM between max and min
        pwm_1 = constrain(pwm_1, PWM_MIN, PWM_MAX);
        pwm_2 = constrain(pwm_2, PWM_MIN, PWM_MAX);

        // send pwm to esc
        esc_1.writeMicroseconds(pwm_1);
        esc_2.writeMicroseconds(pwm_2);

        // logging
        log_data = "";
        log_data += tt;
        log_data += ";";
        log_data += pos1;
        log_data += ";";
        log_data += pos2;
        log_data += ";";
        log_data += speed2;
        log_data += ";";
        log_data += pwm_1;
        log_data += ";";
        log_data += pwm_2;
        log_data += "\n";

}

void checkPos1(){
    if(digitalRead(PINA1_) != digitalRead(PINB1_))
        ++pos1;
    else
        --pos1;
}

void checkPos2(){
    if(digitalRead(PINA2_) != digitalRead(PINB2_))
        ++pos2;
    else
        --pos2;
}
```

APPENDIX A.3: Motor Model Simulation.

```
clc; clear; close all;
%% Motor model


RADPS2RPM = 60/(2*pi);

J = 1.24e-4;
K = 0.0182;
R = 0.83;
%L = 0.1;
b = ( K/54.39 -K^2 )/R;

P = [ b^2 ( -2*b*R*J - 4*K^2*J ) ( R^2*J^2 ) ];

rootsP = roots(P);
L = rootsP(2);
%L = 0.63e-3;

A = [-b/J    K/J
     -K/L    -R/L];
B = [0
     1/L];
C = [1    0];
D = 0;
motor_ss = ss(A, B, C, D);
[bb,aa] = ss2tf(A, B, C, D)
sys_motor = tf( bb, aa )

ii_prev = 0;
OMEGA_prev = 0;
ii_max = 3;

t = 0;
% Simulation Time
T = 10;
% Integration time constant
h = 0.08;
i = 1;

OMEGA_dot = @( OMEGA, ii ) K*ii/J - (b/J)*OMEGA;
ii_dot = @( ii, OMEGA, V ) ( 1/L )*( V - K*OMEGA - R*ii );

tic
while t < T
```

```
    STATE(i,:) = [ t OMEGA_prev*RADPS2RPM ii_prev ];

    Voltage = 8;
    if t >= 5
        Voltage = 0;
    end
    %% Current
    k_1 = ii_dot( ii_prev, OMEGA_prev, Voltage );
    k_2 = ii_dot( ii_prev + 0.5*h*k_1, OMEGA_prev, Voltage );
    k_3 = ii_dot( ii_prev + 0.5*h*k_2, OMEGA_prev, Voltage );
    k_4 = ii_dot( ii_prev + k_3*h, OMEGA_prev, Voltage );

    ii_new = ii_prev + ( 1/6 )*( k_1 + 2*k_2 + 2*k_3 + k_4 )*h;

    if ii_new > ii_max
        ii_new = ii_max;
    elseif ii_new < -ii_max
        ii_new = -ii_max;
    end


    %% Speed
    k_1 = OMEGA_dot( OMEGA_prev, ii_prev );
    k_2 = OMEGA_dot( OMEGA_prev + 0.5*h*k_1, ii_prev );
    k_3 = OMEGA_dot( OMEGA_prev + 0.5*h*k_2, ii_prev );
    k_4 = OMEGA_dot( OMEGA_prev + k_3*h, ii_prev );

    OMEGA_new = OMEGA_prev + ...
        ( 1/6 )*( k_1 + 2*k_2 + 2*k_3 + k_4 )*h;

    % Memory Variable
    ii_prev    = ii_new;
    OMEGA_prev = OMEGA_new;

    i = i + 1;
    t = t + h;
end
toc

%% Current and RPM Plot
figure('Name','RPM');
subplot(2,1,1);
plot( STATE(:,1),STATE(:,2) );
title('RPM')
xlabel('t  (s)')
ylabel('RPM')
grid on
```

```
subplot(2,1,2);
plot( STATE(:,1),STATE(:,3) );
title('Current␣(Amperes)')
xlabel('t␣␣(s)')
ylabel('Current␣(Amperes)')
grid on
```

APPENDIX A.4: Controller Design.

```
clc; clear; close all;
%% Controller Design for Motor model

RADPS2RPM = 60/(2*pi);

J = 1.24e-4;
K_e = 0.0182;
R = 0.83;
L = 0.1;
b = ( K_e/54.39 -K_e^2 )/R;
% Total moment of inertia about Z axis
I = 0.0432 + 0.3*0.145^2;

b_0 = -6.8912e-4*I;
b_1 = 2.0461e-2*I;
b_2 = -5.2491e-2*I;
b_3 = 3.7570e-1*I;

sigma_U = -0.5;
cc = 1;


for K_p = 0:1:100
    for K_d = 0:1:100

        P = [ 1 ( b_2/I + R/L + R*b_2/(I*L) + b/J )...
            ( b*b_2/(I*J) + b*R/(J*L) + (K_e^2)/(J*L)...
            + K_d*K_e/(I*L) ) ( b*R*b_2/(J*L*I)...
            + K_e^2*b_2/(J*L*I) + K_p*K_e/(I*L) ) ];
        rootsP = roots(P);

        for i = 1:3
            real_a(i) = real(rootsP(i));
            imag_a(i) = imag(rootsP(i));
        end
        if real_a(1)<sigma_U && real_a(2)<sigma_U...
                && real_a(3)<sigma_U
            STATE(cc,:) = [ K_p K_d ];
            STATE_Poles(cc,:) = [ real_a(1) imag_a(1)...
                real_a(2) imag_a(2) real_a(3) imag_a(3) ];
            cc = cc + 1;
        end
    end
end
```

```
figure('Name','K_p vs. K_d');
plot( STATE(:,1), STATE(:,2), '.' )
ylabel('K_d')
xlabel('K_p')
%set(gca,'XTick',0:5:T);
title('K_p vs. K_d')
grid on
%  ylim([0 250])
%  xlim([0 210])


figure('Name','Pole Spread');

plot( STATE_Poles(:,1), STATE_Poles(:,2), '.' )
hold on
plot( STATE_Poles(:,3), STATE_Poles(:,4), '.' )
hold on
plot( STATE_Poles(:,5), STATE_Poles(:,6), '.' )
sgrid
ylabel('Imaginary Axis')
xlabel('Real Axis')
%set(gca,'XTick',0:5:T);
title('Pole Spread')

hold off
%  ylim([0 250])
%  xlim([0 210])

k_p = 20;
k_d = 10;
V_MAX = 10;
```

APPENDIX B.1: RW Actuated System Designs

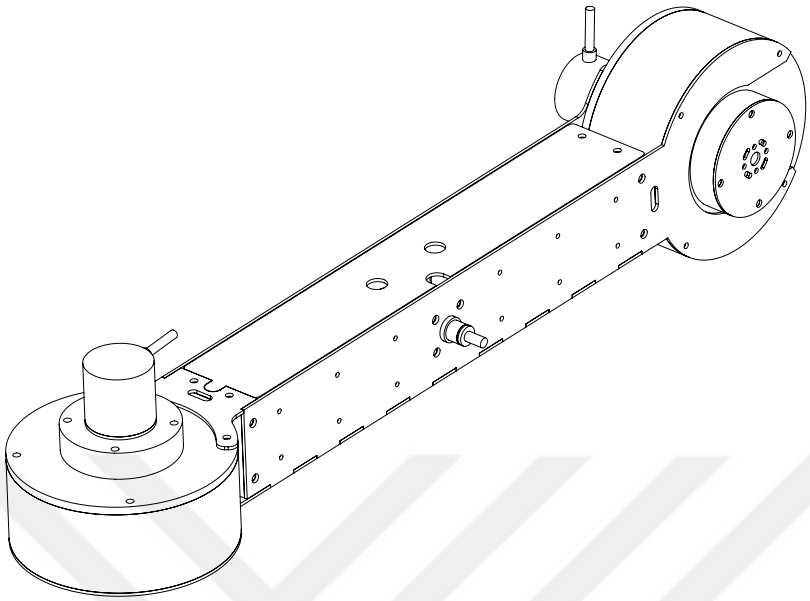

Figure A.1 : The 2DOF RW Actuated Testbed Final Design

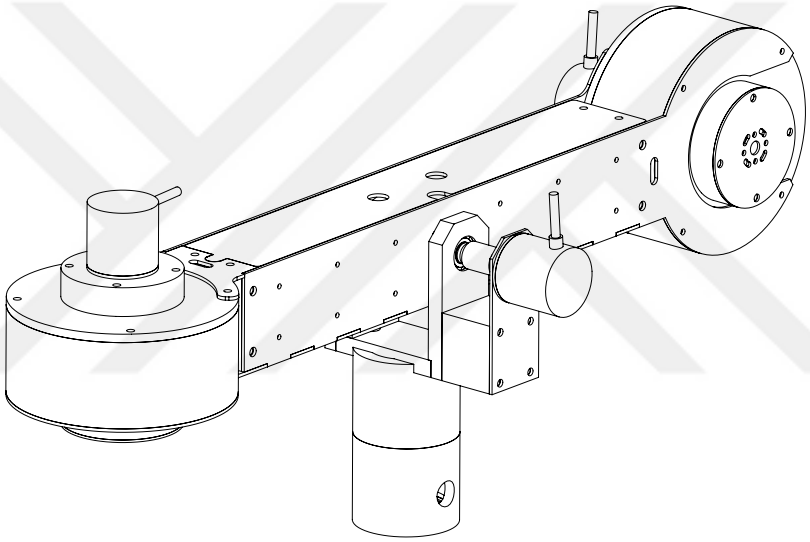

Figure A.2 : The 2DOF RW Actuated Testbed Final Design

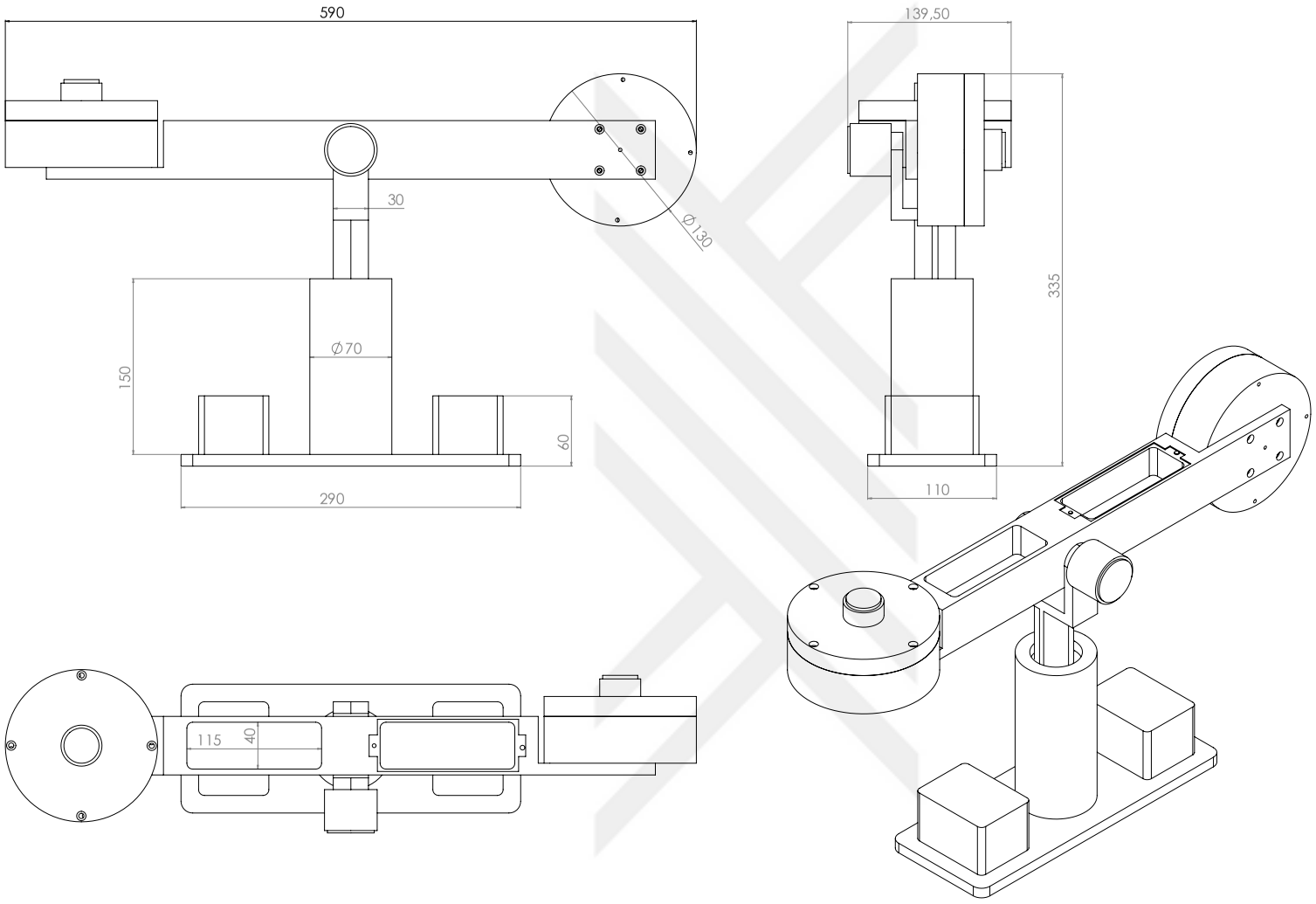

Figure A.3 : The 2DOF RW Actuated Testbed Initial Design

CURRICULUM VITAE

Name Surname: Rahman Bitirgen

Place and Date of Birth: Birecik, 1988

E-Mail: bitirgen@itu.edu.tr

EDUCATION:

- **B.Sc.:** 2016, Istanbul Technical University, Faculty of Aeronautics and Astronautics, Department of Astronautical Engineering
- **M.Sc.:** 2019, Istanbul Technical University, Institute of Sciences, Graduate School of Aeronautics and Astronautics, Department of Aeronautical and Astronautical Engineering

PROFESSIONAL EXPERIENCE AND REWARDS:

- Research and Teaching Assistant - Faculty of Aeronautics and Astronautics, Istanbul Technical University, Istanbul, Turkey, since April 2017
- Researcher - Model Based Design and Control Laboratory, Faculty of Aeronautics and Astronautics, Istanbul Technical University, Istanbul, Turkey, since September 2015

PUBLICATIONS, PRESENTATIONS AND PATENTS ON THE THESIS:

- Bitirgen, R., Bayezit, I., 2018. Time Optimal Control of a Reaction Wheel Actuated System, *The International Conference on Applied Mathematics in Engineering (ICAME'18)*, June 27-29, 2018 Balikesir, Turkey

OTHER PUBLICATIONS, PRESENTATIONS AND PATENTS:

- Bitirgen, R., Bayezit, I., Reyhanoglu, M., 2018. Feedback Linearization Control of a 2DOF Helicopter, *The International Conference on Applied Mathematics in Engineering (ICAME'18)*, June 27-29, 2018 Balikesir, Turkey

- Bitirgen R., Hancer M., Bayezit, I., 2018. All Stabilizing State Feedback Controller for Inverted Pendulum Mechanism, *3rd IFAC Conference on Advances in Proportional-Integral-Derivative Control PID 2018*, May 9-11 Ghent, Belgium.

- Hancer M., Bitirgen R., Bayezit, I., 2018. Designing 3-DOF Hardware-In-The-Loop Test Platform Controlling Multirotor Vehicles, *3rd IFAC Conference on Advances in Proportional-Integral-Derivative Control PID 2018*, May 9-11 Ghent, Belgium.

- Bitirgen R., Bayezit, I., Saldiran E., Mustafa, Y. K., 2016. İki Serbestlik Dereceli Yeniden Şekillendirilebilen Modüler bir Helikopterin Tasarımı, Modellenmesi ve Kontrolü, *TOK2016 Konferansı*, 29 Eylul-1 Ekim Eskisehir, Turkiye.

- Ozturk M., Bitirgen R., Bayezit, I., Ozkol, I., 2016. İki Serbestlik Dereceli Helikopterin Bulanık Mantık Tabanlı Lineer Kuadratik Kontrolü, *TOK2016 Konferansı*, 29 Eylul-1 Ekim Eskisehir, Turkiye.